

Research paper

Synthesis and the interaction of 2-(1*H*-pyrazol-4-yl)-1*H*-imidazo[4,5-*f*][1,10]phenanthrolines with telomeric DNA as lung cancer inhibitors



Jiachun Liu^a, Mei Chen^a, Yanli Wang^a, Xiaoyin Zhao^a, Sijia Wang^a, Yanling Wu^{b, **}, Wen Zhang^{a, *}

^a Lab of Chemical Biology and Molecular Drug Design, College of Pharmaceutical Science, Zhejiang University of Technology, Hangzhou, 310014, China

^b Lab of Molecular Immunology, Virus Inspection Department, Zhejiang Provincial Center for Disease Control and Prevention, Hangzhou, 310051, China

ARTICLE INFO

Article history:

Received 8 December 2016

Received in revised form

4 February 2017

Accepted 15 March 2017

Available online 18 March 2017

Keywords:

Phenanthroline

Lung adenocarcinoma

Antiproliferative activity

Telomeric G-quadruplex

ABSTRACT

A novel series of 2-(1*H*-pyrazol-4-yl)-1*H*-imidazo[4,5-*f*][1,10]phenanthrolines were designed, synthesized and evaluated for their antitumor activity against lung adenocarcinoma by CCK-8 assay, electrophoretic mobility shift assay (EMSA), UV-melting study, wound healing assay and docking study. These compounds showed good inhibitory activities against lung adenocarcinoma. Especially compound **12c** exhibited potential antiproliferative activity against A549 cell line with the half maximal inhibitory concentration (IC₅₀) value of 1.48 μM, which was a more potent inhibitor than cisplatin (IC₅₀ = 12.08 μM) and leading compound **2** (IC₅₀ = 1.69 μM), and the maximum cell inhibitory rate being up to 98.40%. Moreover, further experiments demonstrated that compounds **12a–d** can strongly interact with telomeric DNA to stabilize G-quadruplex DNA with increased Δ*T*_m values from 12.44 to 20.54 °C at a ratio of DNA to compound 1:10. These results implied that growth inhibition of A549 cells mediated by these phenanthroline derivatives is possibly positively correlated to the fact their interaction with telomeric G-quadruplexs.

© 2017 Elsevier Masson SAS. All rights reserved.

1. Introduction

Cancer is a serious public health problem resulting in high morbidity, mortality, and previously incogitable losses in the current world [1]. Lung cancer, a highly invasive and rapidly metastasizing cancer, is the top killer in both men and women, which is classified into two broad histologic classes in terms of their growth and spread differently: small-cell lung carcinomas and non-small cell lung carcinomas (NSCLCs). NSCLC is the most common type that accounts for 80% of lung cancers and includes mainly squamous-cell carcinoma, adenocarcinoma, and large-cell carcinoma [2,3]. At present, the mortality rate remains high for NSCLC patients with relapse occurring within 5 years in 35–50% of patients [4–6], and approximately 15% of patients will have only a 5-

year survival from the time of diagnosis [7].

Despite advances in various treatment strategies including surgery, chemotherapy, radiotherapy, even target therapy over recent decades, some serious problems affect the treatment outcome. Gamma radiotherapy plays a crucial role, but clinical outcome is limited because of radio-resistance resulting from tumor heterogeneity. Conventional chemotherapy plays a major role in the treatment of lung cancer, unfortunately such chemotherapy is limited by the risk of severe toxicity to nearby normal parenchyma, which may result in paralyzed lung function [8]. Cisplatin (DDP) is a well-known chemotherapeutic drug which has been used for treatment of numerous human cancers including bladder, head and neck, lung, ovarian, and testicular cancers, but numerous undesirable effects can't be ignored, such as severe kidney problems, gastrointestinal disorders, allergic reactions, hearing loss, hemorrhage, and lowered immunity leading to infections especially in younger patients [9]. Additionally, NSCLCs tend to be intrinsically resistant to multiple anticancer agents and present acquired resistance to epidermal growth factor receptor tyrosine kinase inhibitors, which is an important problem in the treatment of NSCLC [10,11]. Drug resistance has been observed in many patients who have relapsed from DDP treatment. The DDP-resistant

* Corresponding author. Lab of Chemical Biology and Molecular Drug Design, College of Pharmaceutical Science, Zhejiang University of Technology, 18 Chaowang Road, Hangzhou, 310014, China.

** Corresponding author. Lab of Molecular Immunology, Virus Inspection Department, Zhejiang Provincial Center for Disease Control and Prevention, 630 Xincheng Road, Hangzhou, 310014, China.

E-mail addresses: ywlu@cdc.zj.cn (Y. Wu), wzhang63@zjut.edu.cn (W. Zhang).

A549 variant cells have been undermining the therapeutic effect of drugs because of drug resistance [12]. Thus, there is an urgent need to develop novel anticancer agents that are highly effective and preferentially induce apoptosis of lung cancers rather than normal cells [13].

Human telomeres, special sequences containing (TTAGGG)_n repeats [14–16], are essential structures at the ends of all eukaryotic chromosomes to maintain genome stability and cell proliferation by protecting chromosome ends [17,18]. Nevertheless, telomeres will be shortened gradually in the process of cell differentiation and proliferation, which suggests that cells are destined to senesce and die. Telomerase is a cellular reverse transcriptase which can maintain and repair chromosome integrity and stability through adding telomere repeats to telomere DNA [19], as shown in Fig. 1. In normal cells, the activity of telomerase appears to be quite strictly regulated, except that it can only be detected in stem cells, hematopoietic cells and reproductive cells. However, telomerase is activated and displays vigorous activity in 85–90% cancer cells [20–23], which indicates that telomerase may maintain the length of telomeric DNA and promote the process of cell cycle, so that the cancer cells endow more vitality and inhibit apoptosis in process of proliferation. Hence, inhibiting the activity of telomerase may be a novel strategy for cancer chemotherapy. DNA is the principal genetic molecule in biological systems, especially right handed duplex structural B-DNA. However, DNA structure is polymorphic, a number of non-B DNA secondary structures, such as Z-DNAs, hairpins, cruciforms, and G-quadruplexes, have been found and identified to be unstable and mutagenic [24–26]. G-quadruplexes are important DNA secondary structures formed by stacking G-tetrads in specific G-rich sequences with biological significance, such as human telomeres and oncogene-promoter regions (bcl-2, c-myc, c-kit, k-RAS, PDGF-A, HIF-1 α , VEGF and TK1) [27]. Telomere can fold into G-quadruplex structures through four guanines connected by cyclic Hoogsteen hydrogen bonding of guanine bases in the presence of several cations, which can effectively inhibit the activity of telomerase and promote apoptosis of cancer cells [28–30]. G-quadruplexes play an important role in the cell cycle and control diverse processes, such as telomere maintenance, which suggests that G-quadruplexes have a big potential as targets to develop anticancer agents. However, none of the reported G-quadruplex-interactive small molecules have entered past phase II clinical trials [31]. Therefore, design and discovery of such small molecules that can induce the formation of G-quadruplexes and stabilize the G-quadruplex structures in human telomere has

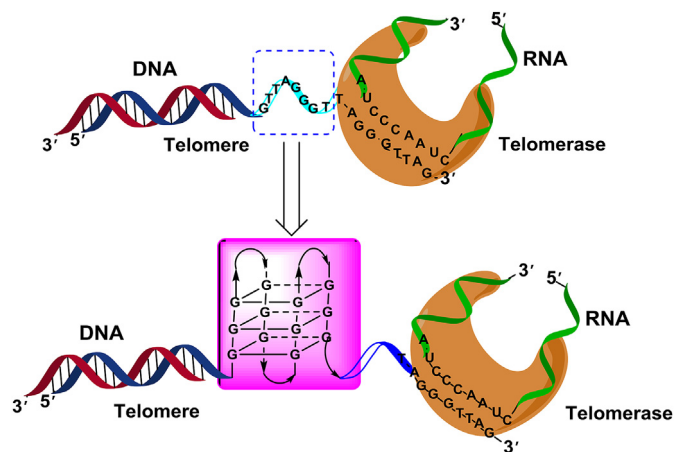
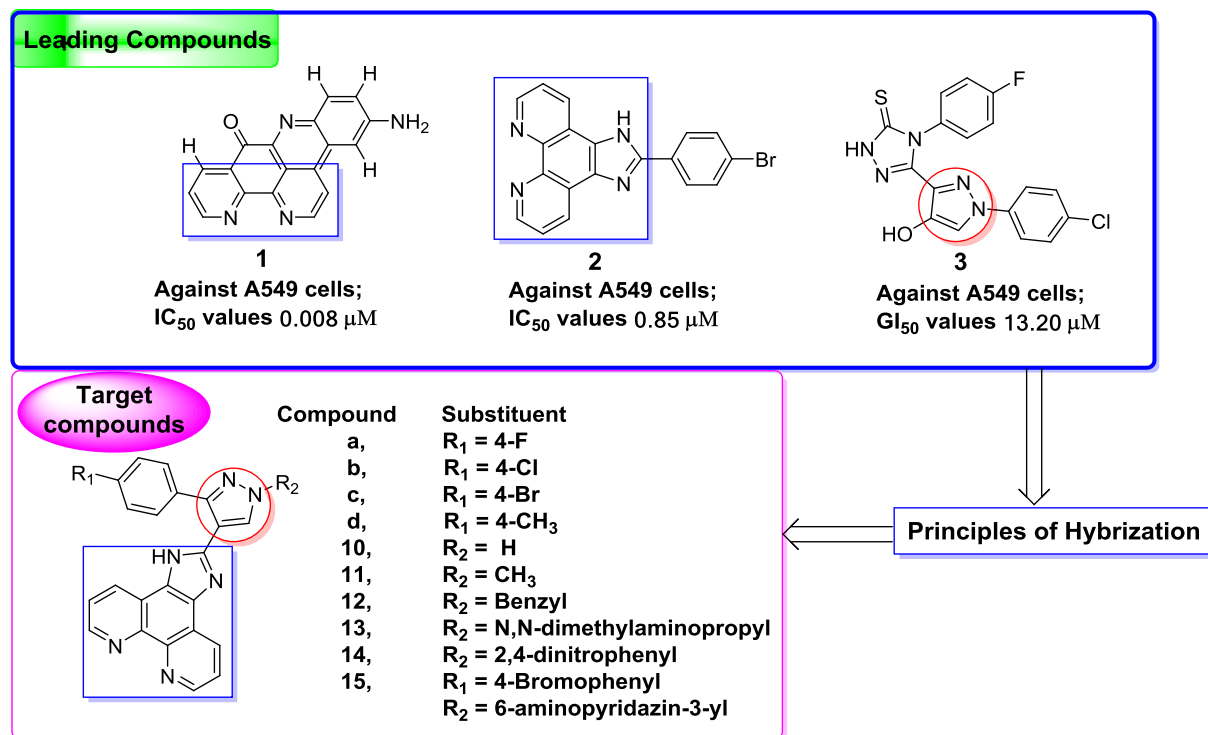


Fig. 1. Telomerase maintains and repairs the length of telomeric DNA. While telomeric DNA forms G-quadruplex structures, the activity of telomerase was inhibited effectively.

become a rational and promising approach in anticancer strategies.

Many nitrogen-containing polycyclic systems are present in a variety of natural and synthetic biologically active agents. Marine compounds with pyridoacridine skeletons have been reported to exhibit interesting antitumor activities. Of which, ascididemin is one of the important examples of these compounds that can damage DNA oxidatively via a thiol-dependent conversion of oxygen to DNA-cleaving radicals [32,33]. As shown in Scheme 1, compound **1**, a substitution product of ascididemin bearing 2,2'-bipyridine moiety, showed good antitumor activity against A549 cells with IC₅₀ value of 8 nM [34]. Likewise, 1,10-phenanthrolines bearing 2,2'-bipyridine moiety are applied importantly in biological sciences, as well as widely in chemistry, physics, and material, which implied that 2,2'-bipyridine moiety seems to have some untapped properties [35–38]. Several mechanisms have elucidated the anticancer activities of 1,10-phenanthrolines, such as the inhibition of DNA synthesis, and G-quadruplex DNA binding property because of the conjugate structure with rigid plane of 1,10-phenanthrolines that can provide a basis for efficient π - π stacking interactions with the terminal G-tetrads [39–41]. In addition, imidazole heterocycles are receiving growing attention with a wide range of applications due to the potency of the imidazole moiety that can be attributed to its hydrogen bond donor-acceptor capability as well as its high affinity for metals, which are presented in many protein active sites [42]. As seen in Scheme 1, compound **2** possessing 1*H*-imidazo[4,5-*f*][1,10]phenanthroline core showed a surprising antitumor activity against A549 cells with IC₅₀ value of 0.85 μ M, which inhibited c-myc gene expression in A549 cells via NF- κ B pathway [43]. Similarly, as the bioisostere of imidazole, pyrazole represents a key structural motif in heterocyclic chemistry and occupies a prominent position in antitumor agents, compound **3** (Scheme 1) showed good activity against A549 cells with the most important GI₅₀ (the concentration for 50% of maximal inhibition of cell proliferation) value of 13.20 μ M [44].

With these results in mind, we designed and synthesized twenty-one novel compounds using a structure-based design strategy using compounds **1**, **2** and **3** as the lead compounds. Based on our previous and other groups' studies [45–47], these small molecules with an extended planar aromatic system can facilitate the stacking action on the G-quartet through π - π interactions, which are similar with a G-quartet in size and shape. 1*H*-imidazo[4,5-*f*][1,10]phenanthroline moiety possesses an extended planar aromatic system, suggesting that the special structure can provide great advantages for the development of small molecules to specifically target G-quadruplexes. Hence, 1*H*-imidazo[4,5-*f*][1,10]phenanthroline moiety was used as key structure skeleton in present work. Furthermore, 1,3-disubstituted pyrazoles were introduced into the imidazole ring at C-2 position to make the synthesized compounds possessing both anti-proliferation activities and stabilized abilities to G-quadruplexes. Detailed designs are shown in Scheme 1. As computer-aided molecular simulation technique is currently regarded as a very useful tool in design of small molecular drugs to expose the interaction mechanism between drugs and biomacromolecules, we, herein, utilized LibDock in Discovery Studio to investigate interactions of compounds (**2** and **12a–d**) with the target G-quadruplex (PDB ID: 3CE5). As shown in Fig. S1, the results illustrated that the phenanthroline skeleton of compounds **12a–d** could mainly stack on the end G-quartet through intermolecular π - π interactions (yellow solid line) and hydrogen bond interaction (green dash line), and the benzyl groups at the N-1 position of pyrazole moiety extended respectively to the groove or loop region of G-quadruplex, both of which could contribute to the stabilization of the G-quadruplex structure. Compounds **12a–d** were mainly adjacent to the residues, such as DG15, DG21, DA2,



Scheme 1. Structure of the leading compounds and design of the target compounds.

DA14, DT13, which were shown in Table 1. However, the *p*-bromophenyl moiety of compound 2 embedded into the groove of G-quadruplex and the imidazole moiety interacted with the base residues (DA2, DG3 and DG21) by hydrogen bonding, not the phenanthroline skeleton interacting with G-quartets, suggesting that the 1,3-disubstituted pyrazole moiety seems to be more advantageous than the *p*-bromophenyl moiety to make the phenanthroline skeleton to stabilize the G-quadruplex in present docking study. These results provided certain theoretical evidence for the following researches.

2. Chemistry

The synthetic route of the 2-(1*H*-pyrazol-4-yl)-1*H*-imidazo[4,5-*f*][1,10]phenanthrolines 10–15 is depicted in Scheme 2. Compounds 4, 5, 9 and 3,6-dichloropyridazine had already been reported in a

previous paper [48–51]. Compounds 6, 7, 8 and 15c were synthesized through the substitution reaction by heating a mixture of compound 4 and iodomethane, (chloromethyl)benzene, 3-dimethylaminopropyl chloride and 3,6-dichloropyridazine under different inorganic base condition in DMF, respectively. Subsequently compound 9 was subjected to a condensation reaction with 4, 5, 6, 7, 8 and 15c in glacial acetic acid (90–100 °C) for 6 h to give the target compounds 10–15, respectively. The structures of the desired compounds were confirmed by ¹H-NMR, a part of ¹³C-NMR, and mass spectral analysis.

3. Results

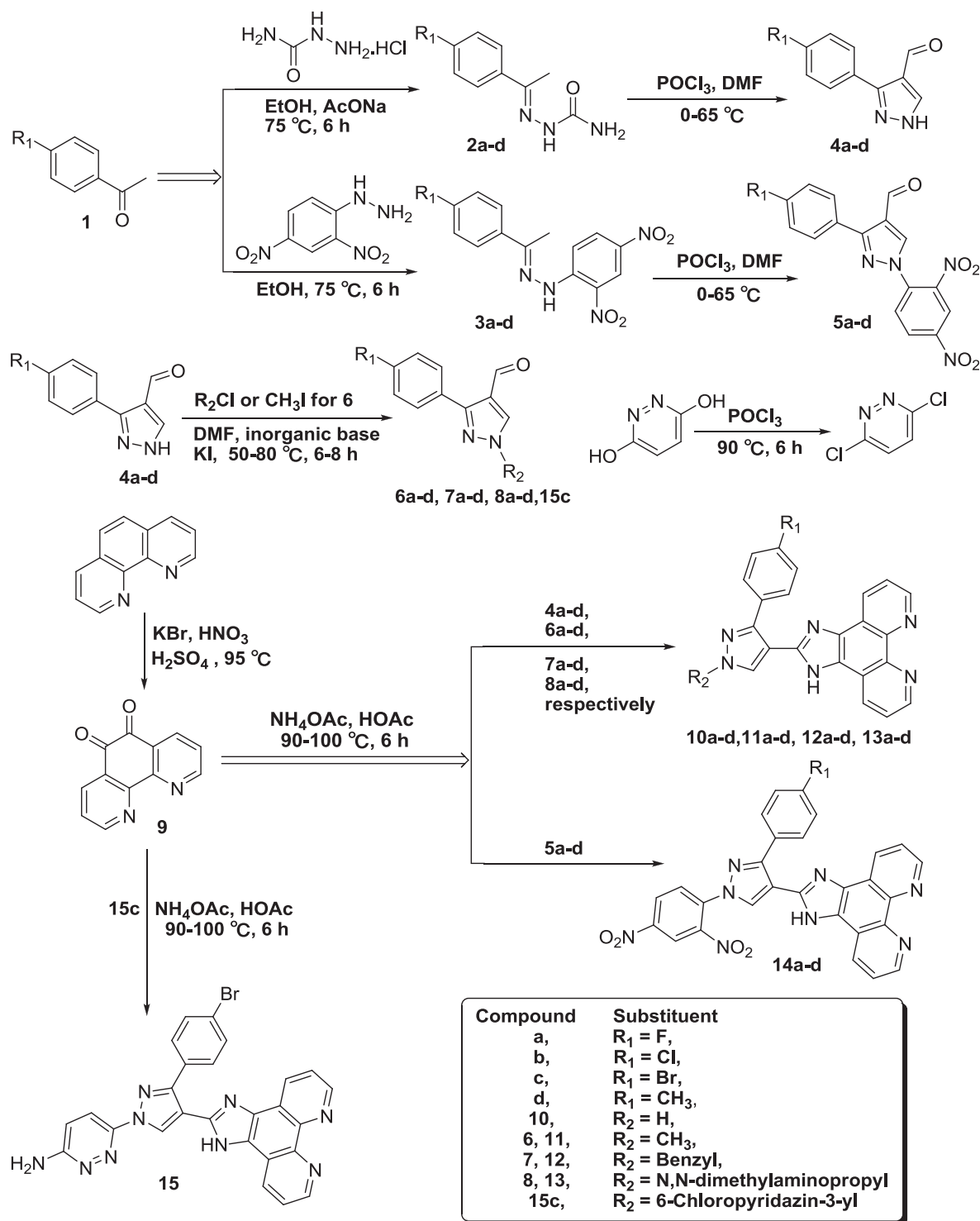
3.1. *In vitro* anti-tumor activity evaluation by CCK-8 assay [52].

To evaluate the antiproliferative abilities of novel synthetic

Table 1

The LibDock scores and docking interactions of compounds (2 and 12a–d) with human telomeric G-quadruplex (PDB ID: 3CE5).

Compound	LibDock score (kcal/mol)	Interacting residues	Interacting atoms
2	89.82	A:DA2:O3'; A:DG3:OP2; B:DG21	Molecule:N15- DG21:H21; Molecule:H32- DG3:OP2; Molecule:H32- DA2:O3'
12a	100.14	B:DG21; B:DG15; B:DG21:O5'	Phenanthroline - DG21, DG15 DG21:O5'-Molecule-H44; DG15:N2-Molecule:N15 DG21-Molecule:N17
12b	84.10	B:DA14; B:DT13; A:DA2	Phenanthroline - DA2, DA14, DT13;
12c	97.89	B:DG21; B:DG15; B:DG21:O5'	Phenanthroline - DG21, DG15; DG15-Molecule:N17; DG21:O5'-Molecule-H43;
12d	100.28	B:DG21; B:DG15; B:DG21:O4'	Pyrazole - DG21; Phenanthroline - DG21; DG21-Molecule-N17 DG21:O4'-Molecule-H43



Scheme 2. Synthetic routes of compounds 10–15.

compounds **10–15** to human lung adenocarcinoma lines (A549 cells) by Cell Counting Kit-8 technique, firstly, A549 cells were treated with 10 μM of compounds **10–15** for 36 h, results of progressive cell growth inhibition were shown in Fig. 2. All compounds exhibited different degrees of antiproliferative activity against A549 cells. Especially, compounds **12a–d** represented the most potent activity at 10 μM , which was stronger than that of cisplatin and leading compound **2**. Secondly, A549 cells were

treated with two-fold serial dilution of cisplatin, leading compound **2**, and **12a–d** for 36 h, respectively. As shown in Fig. 3 and Table 2, compounds **12a–d** presented excellent activity against A549 cells with IC_{50} values in the range of 1.48–2.75 μM . The compound **12c** possessed outstanding antiproliferative activity with IC_{50} value of $1.48 \pm 0.06 \mu\text{M}$, which was almost the same as leading compound **2** ($1.69 \pm 0.07 \mu\text{M}$), but stronger than that of cisplatin ($12.08 \pm 0.41 \mu\text{M}$). Compounds **12a–c** showed stronger activity

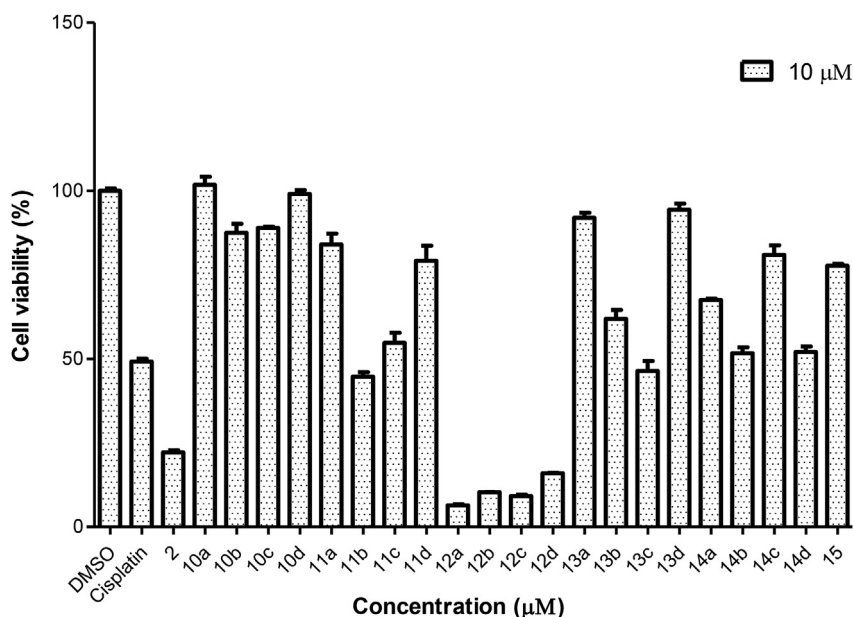


Fig. 2. A549 cells were treated with 10 μM of compounds **10**–**15** for 36 h. Cell viability was determined using Cell Counting Kit-8 assay. Cisplatin and compound **2**: positive controls; DMSO is 1% DMSO solution in RPMI 1640 as a reference.

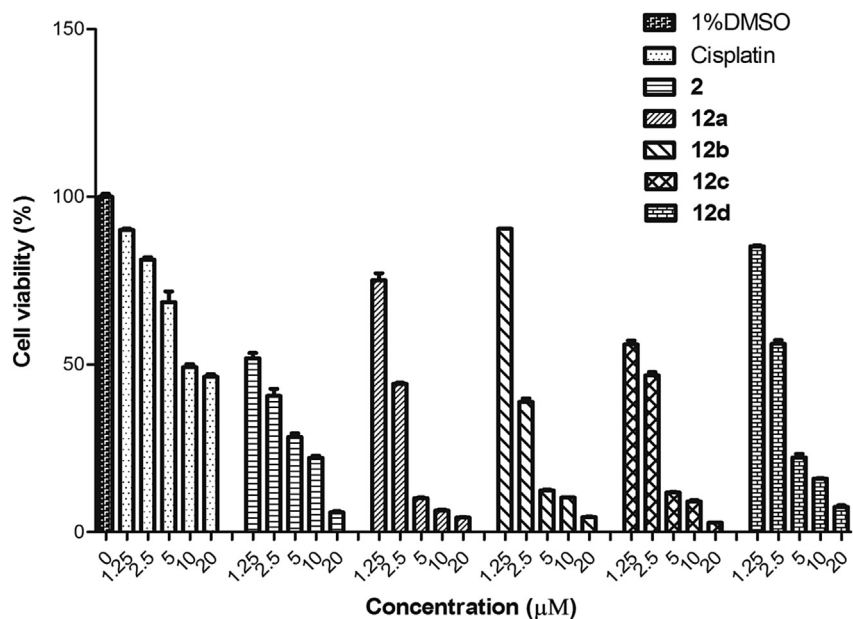


Fig. 3. A549 cells were treated using compounds **12a**–**d** with 0, 1.25, 2.5, 5, 10 and 20 μM for 36 h. Cell viability was determined using Cell Counting Kit-8 assay. Cisplatin and compound **2**: positive control; 0 μM is 1% DMSO solution in RPMI 1640 as a reference.

Table 2
IC₅₀ values (μM) for the A549 and MRC-5 cell lines treated with the desired compounds **12a**–**d** and the positive control drugs (**2** and cisplatin). The values are expressed as the mean \pm SD (triplicates).

Cell line	12a	12b	12c	12d	2	cisplatin
A549	1.78 \pm 0.06 ^a	2.08 \pm 0.03	1.48 \pm 0.06	2.75 \pm 0.09	1.69 \pm 0.07 ^a	12.08 \pm 0.41 ^a
MRC-5	3.80 \pm 0.05 ^a	4.17 \pm 0.03 ^a	3.83 \pm 0.07 ^a	4.76 \pm 0.04 ^a	6.88 \pm 0.01 ^a	21.55 \pm 0.26 ^a
SI ^b	2.13	2.00	2.58	1.73	4.07	1.78

^a Statistically different to lung cancer cell line (A549 and MRC-5) ($P < 0.05$).

^b Selectivity-Index.

than leading compound **2** at 5, 10 and 20 μM , respectively. Unfortunately, the IC₅₀ values of **12a**, **12b** and **12d** were slightly higher

than that of leading compound **2**.

Also, we have carried out the cytotoxicity experiments with

normal human fetal lung fibroblast cells (MRC-5 cells). MRC-5 cells were treated with both positive controls (cisplatin and leading compound **2**) and the desired compounds **12a–d**, under the same conditions. Results were showed in Table 2 and Fig. 4. Compounds **12a–d** presented moderate cytotoxicity against normal MRC-5 cells with IC_{50} values in the range of 3.80–4.76 μ M, which are 1.73–2.58-fold higher than those of A549 cells. Among them, **12c** exhibited the 2.58-fold cytotoxicity against A549 cells over against normal MRC-5 cells, indicating it has definite selectivity for cancer cells, but poor selectivity compared to leading compound **2** with 4.07-fold difference. Collectively, these results suggested that compounds **12a–d** showed excellent cytotoxicity against A549 cells and selectivity to some extent for A549 cells, implying that they may be further explored as leading compounds for cancer inhibitors.

3.2. Preliminary analysis of interaction mechanism by electrophoretic mobility shift assay (EMSA) [45]

In order to explore the cell growth inhibition mechanism, based on our previous study [45] and structural property of compounds with large conjugated and planar aromaticity, we examined the interaction of a serial dilution of compounds (**2** and **12a–d**) with telomeric DNA in Tris buffer (10 mM Tris–HCl, 10 mM KCl, 0.1 mM EDTA, pH = 7.4) by EMSA assay to detect if these compounds have the ability to induce the formation of DNA secondary structures, such as the G-quadruplexes, from the 26nt telomeric G-rich single stranded-DNA sequence containing (GGGTTA)₄ repeats, and

stabilize the DNA-compound complexes. The sequences of newly designed 26nt telomeric DNAs for novel DNA secondary structure formation assay were listed in Table 3, including guanine-rich single stranded-DNA (G-rich DNA), cytosine-rich single stranded-DNA (C-rich DNA) complementary to G-rich DNA, double-stranded DNA (ds-DNA) and Mutated single stranded-DNA (Mut-DNA) with a single G-to-C mutation in the middle of chains of three guanines, impossibly to form any G-quadruplex.

As shown in Fig. 5A–D, EMSA images indicated the interaction of compounds **12a–d** with the G-rich DNA sequences. On gels there are mainly two bands of DNA secondary conformations obviously observed in G-rich DNA: the bright band migrated faster and the fainter band migrated slower roughly at the 20 bp marker level which both may be ascribed to intermolecular G-quadruplexes relative to a double-stranded Marker on the left lane in each gel [53,54]. Based on the EMSA results, **12c** exhibited strongest concentration-dependent interaction with G-quadruplexes, with the bright bands fading away up to 20 μ M, but not compounds **12a**, **12b** and **12d** at the identical concentration level. Likewise, we completed the same investigation with Mut-DNA and ds-DNA sequences as negative controls in the presence of **12c**. Mut-DNA approximately migrated to 15 bp position and ds-DNA displayed normal mobility behaviors (nearly 25 bp) relative to the Marker. No effects of **12c**, even at high concentration levels (40 μ M), on both negative control DNAs were observed in Fig. 5E–F, suggesting that **12c** has strongly specificity for the G-quadruplexes formed in G-rich DNA, a (GGGTTA)₄TT sequence. Likewise, EMSA images of

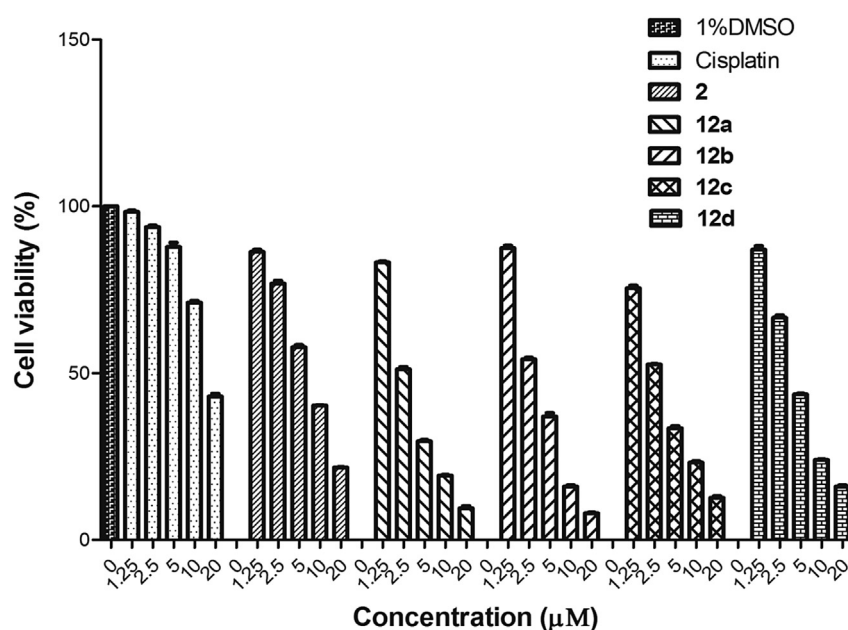


Fig. 4. MRC-5 cells were treated using compounds **12a–d** with 1.25, 2.5, 5, 10 and 20 μ M for 36 h. Cell viability was determined using Cell Counting Kit-8 assay. Cisplatin and compound **2**: positive control; 0 μ M is 1% DMSO solution in DMEM as a reference.

Table 3
The sequences of DNA oligomers used in this study.

Oligomer	Sequence
Tel26nt-G-rich-strand DNA (G-rich DNA)	5'-ttaGGGttaGGGttaGGGttaGGGtt-3'
Tel26nt-C-rich-strand DNA (C-rich DNA)	5'-aaCCctaaCCctaaCCctaaCCctaa-3'
Tel26nt-Mutated-strand DNA (Mut-DNA)	5'-ttaGGGttaGGGttaGGGttaGGGtt-3'
Tel26nt-double-stranded DNA (ds-DNA)	5'-ttaGGGttaGGGttaGGGttaGGGtt-3' 3'-aatCCcaatCCcaatCCcaatCCcaat-5'

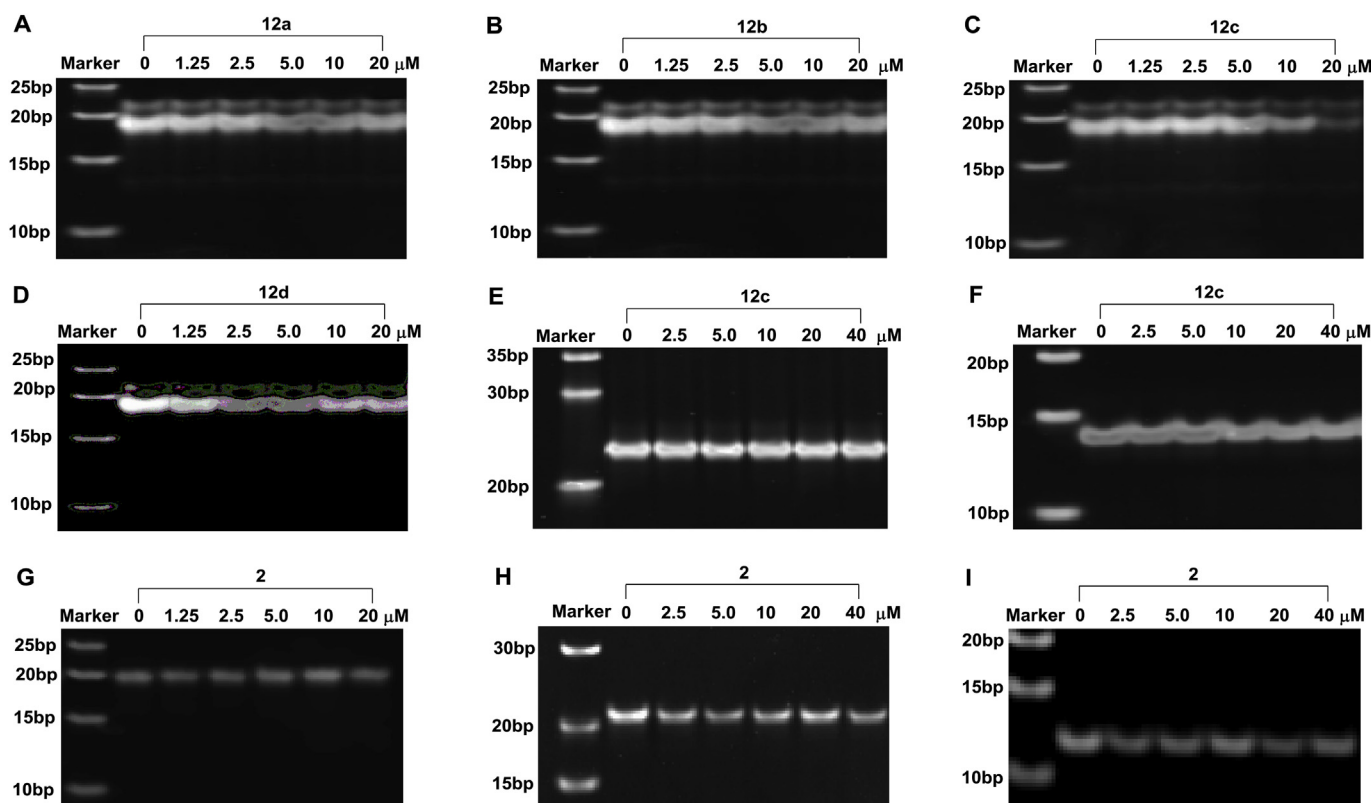


Fig. 5. The ability of phenanthroline derivatives (**2** and **12a–d**) to promote the formation of G-quadruplex structure in the 26nt telomeric DNA sequences. (A–D) EMSA images of Tel26nt G-rich DNA in the presence and absence of **12a–d** at the concentration of 0, 1.25, 2.5, 5, 10, and 20 μM , increasing from left to right. (E) Tel26nt ds-DNA and (F) Tel26nt Mut-DNA were used as negative controls, in which **12c** concentration was ranged from 0 to 40 μM . (G–I) EMSA images of G-rich DNA (G), ds-DNA (H) and Mut-DNA (I) in the presence and absence of **2** concentration was ranged from 0 to 40 μM . Base pairs for used Marker are put on the left side.

leading compound **2** were observed in Fig. 5G–I. In terms of the G-rich DNA sequence, no effects were observed in gels, implied that compound **2** seems unlikely to induce the formation of new DNA secondary structures (Fig. 5G). Similarly, no effects of **2** on both negative control DNAs (ds-DNA and Mut-DNA), even at high concentration levels (40 μM), were observed in Fig. 5H–I.

3.3. Binding of phenanthroline derivatives to telomeric G-quadruplexes [45]

UV-melting study is widely used to determine thermodynamic properties of the folded nucleic acid structures including their stability and interaction with ligands [55,56]. The UV-melting curve of duplex nucleic acids is generally closely related to a hyperchromic shift at 260 nm, while the melting curve of G-quadruplex, i.e. the absorbance of the G-rich DNA decreases with the temperature increasing, with a standard inverted “S” curve presented, is associated with a hypochromic shift at 295 nm [57–58]. Thus, in order to explore binding affinity and mechanism of phenanthroline derivatives with the 26nt telomeric DNAs, the UV absorbance of the nucleic acids was monitored as a function of temperature and then obtained the melting temperature (T_m , °C) that is the mid-point of a melting curve at which the complex is 50% dissociated for quadruplex-forming oligonucleotides in the presence and absence of compounds (**2** and **12a–d**). The tested 26nt telomeric G-rich DNAs for the specific binding assay were listed in Table 3. As shown in Fig. 6A–E and Table 4, the melting curve of the G-rich DNA presented a standard inverted “S” type at 295 nm, which is characteristic of a G-quadruplex structure, suggesting that the G-rich

DNA could form the G-quadruplexes under our experiment conditions. The ΔT_m values, relative to the T_m (39.34 °C) of the G-rich DNA alone, increased greatly from 10.96 °C to 20.54 °C in the presence of compounds (20 μM). Especially, the ΔT_m values of **12a–d** increased higher than that of **2** (10.96 °C) to the G-rich DNA G-quadruplexes. Combined with the present EMSA analysis and previous research [42], no new secondary conformations were observed in the control DNAs, including C-rich DNA, Mut-DNA, ds-DNA, suggesting that the control DNAs were unlikely to form G-quadruplexes under the present experimental conditions.

3.4. Wound healing assay [45].

Cell mobility plays a vital role in tumor metastasis and prognosis of cancer. Therefore, we assessed the effect of compounds (**2** and **12a–d**) on the migration of A549 cells in an *in-vitro* wound healing model. As seen in Fig. S2, an empty space was created with a pipet tip streaked in cell culture, sequentially to culture for 48 h in the presence and absence of compounds (**2** and **12a–d**) and observe the space. The empty space was reduced seriously in size in the absence of compounds because of cell proliferation and migration. The results in Fig. 7 and Table 5 showed that cell inhibitory rates for A549 cells are greater than 16.09% after 48 h treatment with all compounds, while all novel synthesized compounds **12a–d** gave rise to higher cell inhibitory rates for A549 than **2** for target cells at the experimental concentrations. In particular, we observed the fact that compound **12c** was strongest inhibitor to the cell migration with inhibitory rates of 98.40% (± 2.03) for A549 cells. These data are in accord with foregoing EMSA and UV-melting study results

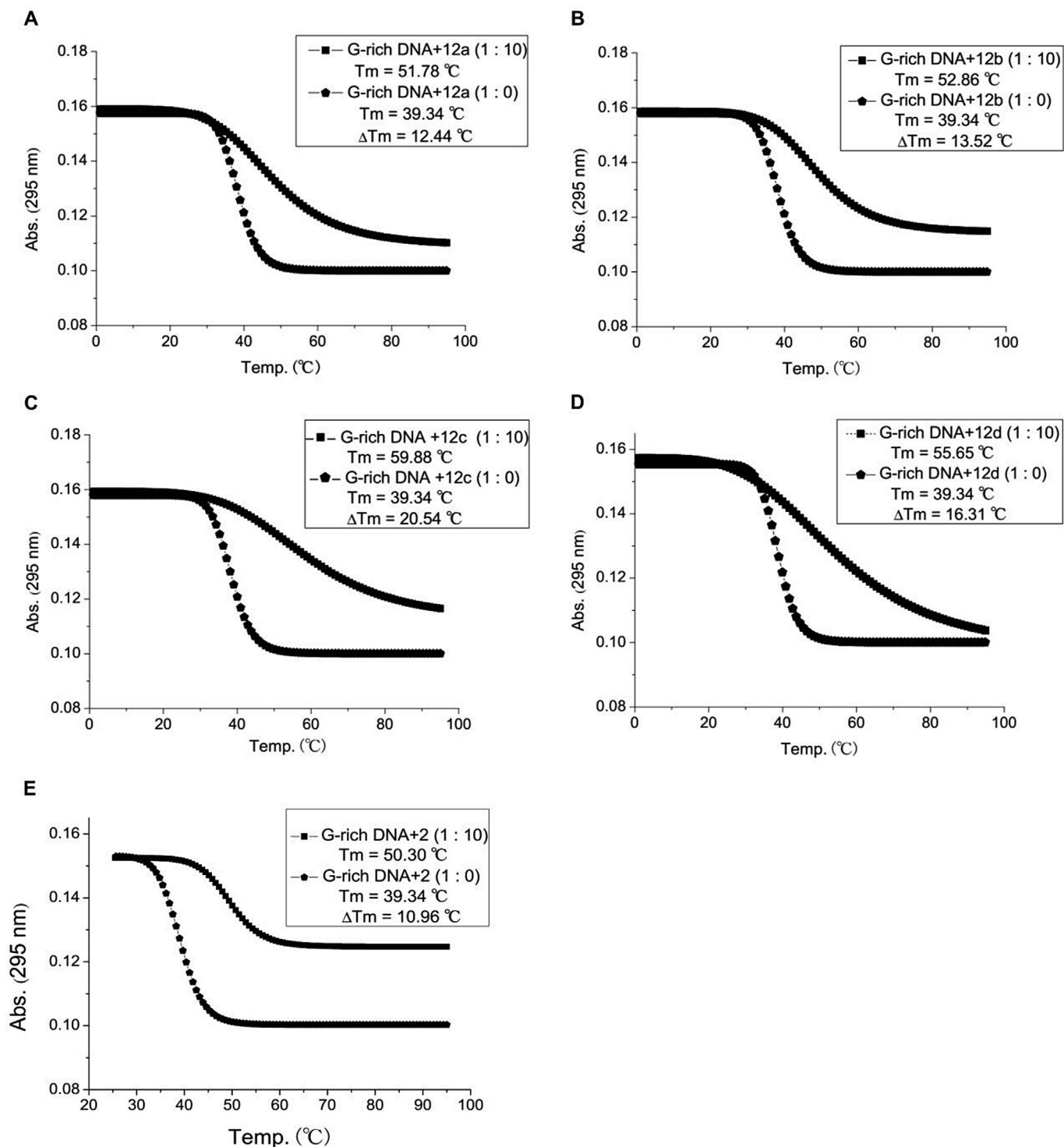


Fig. 6. T_m ($^{\circ}\text{C}$) values for Tel26nt-G-rich-strand DNA (G-rich DNA, 2 μM) interaction with phenanthroline derivatives **12a** (A), **12b** (B), **12c** (C), **12d** (D) and a reference compound **2** (E) at the concentration of 0 and 20 μM , respectively. The ordinate shows the relative absorbance of the samples. The abscissa shows the temperature in $^{\circ}\text{C}$. The melting profiles for the quadruplex formed by the telomeric DNA were acquired at 295 nm.

Table 4

ΔT_m ($^{\circ}\text{C}$) values for Tel-26nt G-rich DNA interaction with phenanthroline derivatives **12a–d**.

	ΔT_m ($^{\circ}\text{C}$) ^a				
	2	12a	12b	12c	12d
G-rich DNA/compound (1:10)	10.96 ± 0.06	12.44 ± 0.07	13.52 ± 1.11	20.54 ± 0.09	16.31 ± 0.05

^a Standard deviation is given.

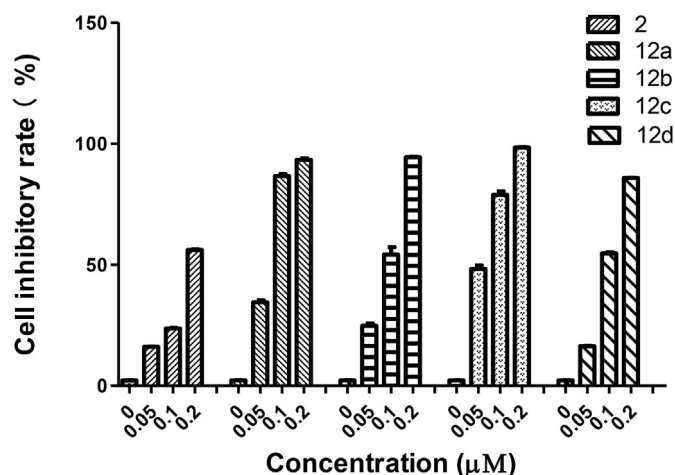


Fig. 7. The bar chart of Cell inhibitory rate (%) for the migration of A549 cells treated with compounds **2** and **12a–d** for 48 h, which showed mean results of three independent experiments in triplicates. The % cell inhibitory rate was calculated by the equation based on the results in Fig. S2: cell inhibitory rate (%) = $(1 - D_{\text{drug}} / D_{\text{control}}) \times 100\%$, where D_{drug} is mean distance of cell migration in drug group, D_{control} is mean distance of cell migration in control group; The % cell inhibitory rate for control is zero. Values are the means \pm S.D. ($P < 0.05$).

and clearly demonstrate that compounds **12a–d** suppressed the mobility of tumor cells.

4. Discussion

Through evaluation of antiproliferative activities of synthesized compounds **10–15** to A549 cells and human normal MRC-5 cells, the results revealed following several structure-activity relationships. Firstly, the antiproliferative activities of compounds **10–15** are not significantly influenced by the R_1 substituent groups on the phenyl ring. Secondly, compounds **12a–d** presented more potent activity than other synthesized compounds, suggesting that *N*-substituted benzyl group at pyrazol moiety seems to play a major role in antiproliferative activity against A549 cells. Compound **12c** showed the best antitumor activity against A549 cells, but had not big difference in the selectivity to MRC-5 cells ($SI = 2.58$), which was better than that of cisplatin ($SI = 1.78$) and weaker than that of compound **2** ($SI = 4.07$). Thirdly, it is particularly encouraging that compounds **12a–d** had better stability ability to human telomere DNA G-quadruplexes based on UV-melting study results, compared to leading compound **2**, which are consistent with docking studies, suggesting that the 1-benzyl-3-phenyl-1*H*-pyrazole moiety could be more advantageous than the *p*-bromophenyl moiety to make the phenanthroline skeleton, and also π - π interactions seem to be more effective than hydrogen bonding interaction to stabilize DNA G-quadruplexes. Similarly, the inhibitory effects of **12a–d** on the mobility of A549 cells were more significant than that of compound **2** under the same condition, implied that the introduction of 1-benzyl-3-phenyl-1*H*-pyrazole moiety to phenanthroline skeleton was successful.

Table 5

Cell inhibitory rate (%) for the migration of A549 cells treated with compounds (**2** and **12a–d**) for 48 h. Values are evaluated with the mean of triplicates.

Concentration	Cell inhibitory rate (%) ^a				
	2	12a	12b	12c	12d
0.05 μM	16.09 ± 0.86	34.46 ± 0.99	24.72 ± 1.19	48.31 ± 2.03	16.34 ± 1.02
0.1 μM	23.67 ± 1.15	86.57 ± 3.04	54.18 ± 1.26	78.81 ± 1.07	54.65 ± 2.34
0.2 μM	56.11 ± 1.66	93.32 ± 2.10	94.41 ± 2.86	98.40 ± 2.03	85.77 ± 2.16

^a Standard deviation is given.

5. Conclusion

Taken together, these findings provided reasonable evidences that all the new synthesized compounds possessed potent anti-proliferative activity against A549 cells. Compounds **12a–d** showed stronger inhibitory activities with IC_{50} values in the range of 1.48–2.75 μM, especially compound **12c** did the strongest against A549 cell line with IC_{50} value of 1.48 μM, which was even more potent than cisplatin ($IC_{50} = 12.08$ μM) and leading compound **2** ($IC_{50} = 1.69$ μM). Moreover, compounds **12a–d** exhibited significant interactions with telomere 26nt G-rich DNA to stabilize the G-quadruplexes based on docking and UV-melting study results, hinting that these evaluated compounds can inhibit the proliferation of A549 cells greatly possibly through interacting with the 26nt telomeric G-quadruplexes, but further mechanism need to be further explored. Similarly, the inhibitory effects of **12a–d** on the mobility of A549 cells were outstanding, indicating that phenanthrolines bearing 1-benzyl-3-phenyl-1*H*-pyrazole moiety could inhibit effectively lung cancer invasion and metastasis. All in all, the study has demonstrated that the imidazo[4,5-*f*][1,10]phenanthrolines containing the 1,3-substituted pyrazol moiety could be further developed as new inhibitors against A549 cells and provide theory basis supporting for phenanthroline drug development.

6. Experimental protocols

6.1. Chemistry

All solvents and chemicals were analytic pure, used without further purification, and obtained from commercial suppliers. However, phosphorus oxychloride and dimethyl formamide (DMF) were further dried by vacuum distillation based on the conditions of Vilsmeier-Haack reaction. The melting points of compounds were observed on the melting point detector (XT-5A). Reaction processes were tracked by TLC on silica gel-precoated F254 Merck plates and the thin layer plates were examined under the UV lamps (254 nm and 365 nm). ¹H-NMR spectra were recorded in pure DMSO-*d*₆ on Bruker NMR spectrometers (AVANCEIII500MHz) using tetramethylsilane (TMS) as internal standard. Chemical shifts were expressed in δ , ppm. Mass spectra were measured on an Agilent 6210 TOF LC/MS (USA).

6.1.1. General synthetic procedure for the key intermediates **6a–d**

To a solution of compounds **4a–d** (1.0 mmol) and iodomethane (0.14 g, 1.0 mmol) in 10.0 ml DMF were added potassium carbonate (0.14 g, 1.0 mmol). The reaction mixture was stirred at 50–60 °C for 4–6 h until the completion of the reaction checked by thin-layer chromatography (TLC). The resulting reaction mixture was poured into 50 mL water, stirred for 5 min, extracted with ethyl acetate (3 \times 40 mL), dried with Na₂SO₄, filtered, concentrated and finally purified by silica gel chromatography (dichloromethane/*n*-hexane, 60:1) to afford pure white crystals **6a–d**. The yield, melting point and spectral data of each compound are given below.

6.1.1.1. *3-(4-fluorophenyl)-1-methyl-1H-pyrazole-4-carbaldehyde (6a)*. White crystal; yield: 66.6%; m.p. 98–100 °C. ¹H-NMR (CDCl₃-d₁, 500 MHz, ppm): δ9.909 (s, 1H, CHO-H), 7.990 (s, 1H, CH), 7.767–7.727 (m, 2H, Ph-H), 7.179–7.133 (m, 2H, Ph-H), 3.993 (s, 3H, CH₃).

6.1.1.2. *3-(4-chlorophenyl)-1-methyl-1H-pyrazole-4-carbaldehyde (6b)*. White crystal; yield: 68.4%; m.p. 87–89 °C. ¹H-NMR (DMSO-d₆, 500 MHz, ppm): δ9.857 (s, 1H, CHO-H), 8.548 (s, 1H, CH), 7.903–7.876 (m, 2H, Ph-H), 7.536–7.509 (m, 2H, Ph-H), 3.961 (s, 3H, CH₃).

6.1.1.3. *3-(4-bromophenyl)-1-methyl-1H-pyrazole-4-carbaldehyde (6c)*. White crystal; yield: 70.1%; m.p. 89–91 °C. ¹H-NMR (CDCl₃-d₁, 500 MHz, ppm): δ9.915 (s, 1H, CHO-H), 7.995 (s, 1H, CH), 7.666–7.641 (m, 2H, Ph-H), 7.608–7.583 (m, 2H, Ph-H), 3.996 (s, 3H, CH₃).

6.1.1.4. *1-Methyl-3-(p-tolyl)-1H-pyrazole-4-carbaldehyde (6d)*. White crystal; yield: 70.1%; m.p. 86–88 °C. ¹H-NMR (CDCl₃-d₁, 500 MHz, ppm): δ9.931 (s, 1H, CHO-H), 7.986 (s, 1H, CH), 7.609–7.593 (d, J₁ = 8.0 Hz, 2H, Ph-H), 7.286–7.270 (d, J₁ = 8.0 Hz, 2H, Ph-H), 3.988 (s, 3H, CH₃), 2.411 (s, 3H, CH₃).

6.1.2. General synthetic procedure for the key intermediates 7a–d

A solution of compounds **4a–d** (1.0 mmol) in DMF (10 mL) was added potassium carbonate (0.15 g, 1.1 mmol) and (chloromethyl) benzene (0.14 g, 1.1 mmol), respectively. The reaction was catalyzed with potassium iodide with stirring at 50 °C for 5–6 h. The reaction was monitored by TLC for completion. The resulting reaction mixture was poured into 50 mL water, stirred for 5 min, extracted with ethyl acetate (3 × 40 mL), dried with Na₂SO₄, filtered, concentrated and finally purified by silica gel chromatography (dichloromethane/n-hexane, 15:1) to afford pure colorless liquid **7a–d**. The yield, melting point and spectral data of each compound are given below.

6.1.2.1. *1-Benzyl-3-(4-fluorophenyl)-1H-pyrazole-4-carbaldehyde (7a)*. Colorless liquid; yield: 73.7%. ¹H-NMR (DMSO-d₆, 500 MHz, ppm): δ9.868 (s, 1H, CHO-H), 8.695 (s, 1H, CH), 7.916–7.875 (m, 2H, Ph-H), 7.407–7.357 (m, 4H, Ph-H), 7.350–7.316 (m, 1H, Ph-H), 7.307–7.259 (m, 2H, Ph-H), 5.455 (s, 2H, CH₂).

6.1.2.2. *1-Benzyl-3-(4-chlorophenyl)-1H-pyrazole-4-carbaldehyde (7b)*. Colorless liquid; yield: 76.6%. ¹H-NMR (DMSO-d₆, 500 MHz, ppm): δ9.886 (s, 1H, CHO-H), 8.717 (s, 1H, CH), 7.900–7.872 (m, 2H, Ph-H), 7.528–7.501 (m, 2H, Ph-H), 7.410–7.363 (m, 4H, Ph-H), 7.358–7.318 (m, 1H, Ph-H), 5.466 (s, 2H, CH₂).

6.1.2.3. *1-Benzyl-3-(4-bromophenyl)-1H-pyrazole-4-carbaldehyde (7c)*. Colorless liquid; yield: 85.29%. ¹H-NMR (DMSO-d₆, 500 MHz, ppm): δ9.890 (s, 1H, CHO-H), 8.721 (s, 1H, CH), 7.834–7.807 (m, 2H, Ph-H), 7.665–7.637 (m, 2H, Ph-H), 7.408–7.371 (m, 4H, Ph-H), 7.352–7.321 (m, 1H, Ph-H), 5.468 (s, 2H, CH₂).

6.1.2.4. *1-Benzyl-3-(p-tolyl)-1H-pyrazole-4-carbaldehyde (7d)*. Colorless liquid; yield: 69.2%. ¹H-NMR (DMSO-d₆, 500 MHz, ppm): δ9.863 (s, 1H, CHO-H), 8.649 (s, 1H, CH), 7.703–7.687 (m, 2H, Ph-H), 7.400–7.328 (m, 5H, Ph-H), 7.268–7.252 (m, 2H, Ph-H), 5.438 (s, 2H, CH₂), 2.345 (s, 3H, CH₃).

6.1.3. General synthetic procedure for the key intermediates 8a–d

A solution of compounds **4a–d** (10.0 mmol) in DMF (15 mL) was added sodium hydride (0.72 g, 30.0 mmol) with stirring at room temperature for 0.5 h. Then, 3-dimethylaminopropyl chloride

hydrochloride (1.73 g, 11.0 mmol) was added to the reaction mixture. Further, the mixture was stirred at 70 °C for 5–8 h in the presence of the catalyst potassium iodide. Once the reaction finished, the mixture was poured into ice water and extracted with ethyl acetate (3 × 40 mL), dried with Na₂SO₄, filtered, concentrated and finally purified by silica gel chromatography (dichloromethane/methanol, 40:1) to afford pure yellow liquid **8a–d**. The yield, melting point and spectral data of each compound are given below.

6.1.3.1. *1-(3-(dimethylamino)propyl)-3-(4-fluorophenyl)-1H-pyrazole-4-carbaldehyde (8a)*. Yellow liquid; yield: 44.2%. ¹H-NMR (CDCl₃-d₁, 500 MHz, ppm): δ9.909 (s, 1H, CHO-H), 8.057 (s, 1H, CH), 7.790–7.750 (m, 2H, Ph-H), 7.173–7.126 (m, 2H, Ph-H), 4.281–4.254 (t, J₁ = 6.75 Hz, 2H, CH₂), 2.325–2.297 (t, J₁ = 7.0 Hz, 2H, CH₂), 2.251 (s, 6H, CH₃), 2.131–2.076 (m, 2H, CH₂).

6.1.3.2. *3-(4-chlorophenyl)-1-(3-(dimethylamino)propyl)-1H-pyrazole-4-carbaldehyde (8b)*. Yellow liquid; yield: 46.8%. ¹H-NMR (CDCl₃-d₁, 500 MHz, ppm): δ9.921 (s, 1H, CHO-H), 8.125 (s, 1H, CH), 7.750–7.724 (m, 2H, Ph-H), 7.450–7.423 (m, 2H, Ph-H), 4.351–4.324 (t, J₁ = 6.75 Hz, 2H, CH₂), 2.539–2.514 (t, J₁ = 6.25 Hz, 2H, CH₂), 2.417 (s, 6H, CH₃), 2.268–2.214 (m, 2H, CH₂).

6.1.3.3. *3-(4-bromophenyl)-1-(3-(dimethylamino)propyl)-1H-pyrazole-4-carbaldehyde (8c)*. Yellow liquid; yield: 47.7%. ¹H-NMR (CDCl₃-d₁, 500 MHz, ppm): δ9.817 (s, 1H, CHO-H), 7.970 (s, 1H, CH), 7.605–7.579 (m, 2H, Ph-H), 7.501–7.474 (m, 2H, Ph-H), 4.183–4.155 (t, J₁ = 7.0 Hz, 2H, CH₂), 2.213–2.186 (t, J₁ = 6.75 Hz, 2H, CH₂), 2.146 (s, 6H, CH₃), 2.024–1.970 (m, 2H, CH₂).

6.1.3.4. *1-(3-(dimethylamino)propyl)-3-(p-tolyl)-1H-pyrazole-4-carbaldehyde (8d)*. Yellow liquid; yield: 39.5%. ¹H-NMR (CDCl₃-d₁, 500 MHz, ppm): δ9.858 (s, 1H, CHO-H), 7.973 (s, 1H, CH), 7.546–7.530 (m, 2H, Ph-H), 7.195 (br. s, 2H, Ph-H), 4.206–4.178 (t, J₁ = 7.0 Hz, 2H, CH₂), 2.338 (s, 3H, CH₃), 2.262–2.234 (t, J₁ = 7.0 Hz, 2H, CH₂), 2.185 (s, 6H, CH₃), 2.066–2.011 (m, 2H, CH₂).

6.1.4. General synthetic procedure for the key intermediate 15c

Firstly, a mixture of maleic hydrazide (8.9 mmol, 1.0 g) and phosphorus oxychloride (15 mL) was heated at 90 °C for 6 h to afford 3,6-dichloropyridazine, purified by silica gel chromatography (dichloromethane/n-hexane, 15:1) to afford white crystals. Secondly, a solution of compound **4c** (2.50 g, 10.0 mmol) in DMF (10 mL) was added sodium hydride (0.24 g, 10.0 mmol) and newly synthetic 3,6-dichloropyridazine (1.63 g, 11.0 mmol), respectively. The reaction was stirred at 70 °C for 10 h in the presence of a catalyst potassium iodide and monitored by TLC for completion. The resulting reaction mixture was poured into 50 mL water and stirred for 5 min, extracted with ethyl acetate (3 × 40 mL), dried with Na₂SO₄, filtered, concentrated and finally purified by silica gel chromatography (dichloromethane as the mobile phase) to afford white product **15c**. The yield, melting point and spectral data of each compound are given below.

6.1.4.1. *3-(4-bromophenyl)-1-(6-chloropyridazin-3-yl)-1H-pyrazole-4-carbaldehyde (15c)*. White product; yield: 59.6%. ¹H-NMR (DMSO-d₆, 500 MHz, ppm): δ 10.082 (s, 1H, CHO-H), 9.648 (s, 1H, CH), 8.447–8.429 (d, J₁ = 9.0 Hz, 1H, Pyridazine-H), 8.211–8.192 (d, J₁ = 9.5 Hz, 1H, Pyridazine-H), 8.004–7.978 (m, 2H, Ph-H), 7.749–7.722 (m, 2H, Ph-H).

6.1.5. General procedure for the target compounds 10–15

A mixture of 1,10-phenanthroline-5,6-dione **9** (0.10 g, 0.48 mmol), ammonium acetate (0.4 g, 5.19 mmol), 0.50 mmol

(**4a–d**, **5a–d**, **6a–d**, **7a–d**, **8a–d** and **15c**, respectively) in glacial acetic acid (20 mL) was heated and stirred at 90 °C under purified nitrogen atmosphere for 6 h. The reaction was monitored by TLC for completion. The resultant solution was concentrated and neutralized with concentrated aqueous ammonia. The yellow precipitate was collected, washed with water and purified by silica gel chromatography (dichloromethane/methanol, 15:1) to afford pure yellow products (**10a–d**, **14a–d** and **15**), white crystals (**11a–d**, **12a–d** and **13a–d**), respectively. The yield, melting point, purity and spectral data of each compound are given below.

6.1.5.1. 2-(3-(4-fluorophenyl)-1H-pyrazol-4-yl)-1H-imidazo[4,5-f][1,10]phenanthroline (10a). Yellow solid; yield: 78.8%; m.p. 272–274 °C; purity by HPLC: 97.2%. ¹H-NMR (DMSO-*d*₆, 500 MHz, ppm): δ13.534 (br. s, 2H, NH), 9.041–9.029 (dd, *J*₁ = 4.5 Hz, *J*₂ = 2.0 Hz, 2H, Phenanthroline-H), 8.837–8.822 (d, *J*₁ = 7.5 Hz, 2H, Phenanthroline-H), 8.380 (br. s, 1H, CH), 8.096–8.068 (dd, *J*₁ = 8.0 Hz, *J*₂ = 6.0 Hz, 2H, Ph-H), 7.853–7.828 (dd, *J*₁ = 8.0 Hz, *J*₂ = 4.5 Hz, 2H, Phenanthroline-H), 7.312 (br. s, 2H, Ph-H). MS (ESI) calcd for C₂₂H₁₃FN₆: 380.12, found: 381.1 (M + H⁺).

6.1.5.2. 2-(3-(4-chlorophenyl)-1H-pyrazol-4-yl)-1H-imidazo[4,5-f][1,10]phenanthroline (10b). Yellow solid; yield: 81.2%; m.p. 285–287 °C; purity by HPLC: 96.6%. ¹H-NMR (DMSO-*d*₆, 500 MHz, ppm): δ13.551–13.531 (d, *J*₁ = 10 Hz, 2H, NH), 9.039–9.027 (dd, *J*₁ = 4.0 Hz, *J*₂ = 1.5 Hz, 2H, Phenanthroline-H), 8.824 (br. s, 2H, Phenanthroline-H), 8.486 (br. s, 1H, CH), 8.067 (br. s, 2H, Ph-H), 7.830 (br. s, 2H, Phenanthroline-H), 7.622 (br. s, 1H, Ph-H), 7.493–7.481 (d, *J*₁ = 6.0 Hz, 1H, Ph-H). MS (ESI) calcd for C₂₂H₁₃ClN₆: 396.09, found: 397.1 (M + H⁺).

6.1.5.3. 2-(3-(4-bromophenyl)-1H-pyrazol-4-yl)-1H-imidazo[4,5-f][1,10]phenanthroline (10c). Yellow solid; yield: 84.6%; m.p. 279–281 °C; purity by HPLC: 95.8%. ¹H-NMR (DMSO-*d*₆, 500 MHz, ppm): δ13.722 (br. s, 1H, NH), 13.614 (br. s, 1H, NH), 9.052–9.041 (dd, *J*₁ = 4.0 Hz, *J*₂ = 1.5 Hz, 2H, Phenanthroline-H), 8.848 (br. s, 2H, Phenanthroline-H), 8.533 (br. s, 1H, CH), 8.045–8.030 (d, *J*₁ = 7.5 Hz, 2H, Ph-H), 7.851–7.826 (dd, *J*₁ = 8.0 Hz, *J*₂ = 4.5 Hz, 2H, Phenanthroline-H), 7.750 (br. s, 1H, Ph-H), 7.646 (br. s, 1H, Ph-H). MS (ESI) calcd for C₂₂H₁₃BrN₆: 440.04, found: 440.1 (M + H⁺).

6.1.5.4. 2-(3-(*p*-tolyl)-1H-pyrazol-4-yl)-1H-imidazo[4,5-f][1,10]phenanthroline (10d). Yellow solid; yield: 78.3%; m.p. 264–266 °C; purity by HPLC: 96.3%. ¹H-NMR (DMSO-*d*₆, 500 MHz, ppm): δ13.549 (br. s, 2H, NH), 9.036 (br. s, 2H, Phenanthroline-H), 8.846–8.832 (d, *J*₁ = 6.0 Hz, 2H, Phenanthroline-H), 8.237 (br. s, 1H, CH), 7.887 (br. s, 2H, Ph-H), 7.835–7.820 (m, 2H, Phenanthroline-H), 7.268 (br. s, 2H, Ph-H), 2.345 (s, 3H, CH₃). MS (ESI) calcd for C₂₃H₁₆N₆: 376.14, found: 377.1 (M + H⁺).

6.1.5.5. 2-(3-(4-fluorophenyl)-1-methyl-1H-pyrazol-4-yl)-1H-imidazo[4,5-f][1,10]phenanthroline (11a). White crystal; yield: 85.3%; m.p. >310 °C; purity by HPLC: 98.4%. ¹H-NMR (DMSO-*d*₆, 500 MHz, ppm): δ13.514 (br. s, 1H, NH), 9.034–9.022 (dd, *J*₁ = 4.5 Hz, *J*₂ = 2.0 Hz, 2H, Phenanthroline-H), 8.825–8.809 (d, *J*₁ = 8.0 Hz, 1H, Phenanthroline-H), 8.779–8.763 (d, *J*₁ = 8.0 Hz, 1H, Phenanthroline-H), 8.394 (s, 1H, CH), 8.037–7.996 (m, 2H, Ph-H), 7.843–7.798 (m, 2H, Phenanthroline-H), 7.268–7.220 (m, 2H, Ph-H), 4.039 (s, 3H, CH₃). MS (ESI) calcd for C₂₃H₁₅FN₆: 394.13, found: 395.2 (M + H⁺).

6.1.5.6. 2-(3-(4-chlorophenyl)-1-methyl-1H-pyrazol-4-yl)-1H-imidazo[4,5-f][1,10]phenanthroline (11b). White crystal; yield: 84.7%; m.p. >310 °C; purity by HPLC: 97.1%. ¹H-NMR (DMSO-*d*₆, 500 MHz, ppm): δ13.526 (br. s, 1H, NH), 9.037–9.025 (dd, *J*₁ = 4.5 Hz,

*J*₂ = 2.0 Hz, 2H, Phenanthroline-H), 8.835–8.821 (d, *J*₁ = 7.0 Hz, 1H, Phenanthroline-H), 8.781–8.766 (d, *J*₁ = 7.5 Hz, 1H, Phenanthroline-H), 8.409 (s, 1H, CH), 8.032–8.004 (m, 2H, Ph-H), 7.847–7.799 (m, 2H, Phenanthroline-H), 7.490–7.463 (m, 2H, Ph-H), 4.046 (s, 3H, CH₃). MS (ESI) calcd for C₂₃H₁₅ClN₆: 410.10, found: 411.1 (M + H⁺).

6.1.5.7. 2-(3-(4-bromophenyl)-1-methyl-1H-pyrazol-4-yl)-1H-imidazo[4,5-f][1,10]phenanthroline (11c). White crystal; yield: 86.4%; m.p. >310 °C; purity by HPLC: 96.9%. ¹H-NMR (DMSO-*d*₆, 500 MHz, ppm): δ9.014–9.010 (d, *J*₂ = 2.0 Hz, 2H, Phenanthroline-H), 8.838–8.823 (d, *J*₁ = 7.5 Hz, 2H, Phenanthroline-H), 8.498 (s, 1H, CH), 8.022–8.006 (d, *J*₁ = 8.0 Hz, 2H, Ph-H), 7.824–7.801 (m, 2H, Phenanthroline-H), 7.623–7.607 (d, *J*₁ = 8.0 Hz, 2H, Ph-H), 4.024 (s, 3H, CH₃). MS (ESI) calcd for C₂₃H₁₅BrN₆: 454.05, found: 455.1 (M + H⁺).

6.1.5.8. 2-(1-Methyl-3-(*p*-tolyl)-1H-pyrazol-4-yl)-1H-imidazo[4,5-f][1,10]phenanthroline (11d). White crystal; yield: 81.1%; m.p. >310 °C; purity by HPLC: 97.4%. ¹H-NMR (DMSO-*d*₆, 500 MHz, ppm): δ13.525 (s, 1H, NH), 9.034–9.022 (dd, *J*₁ = 4.5 Hz, *J*₂ = 2.0 Hz, 2H, Phenanthroline-H), 8.805–8.802 (m, 2H, Phenanthroline-H), 8.360 (s, 1H, CH), 7.823–7.790 (m, 4H, Ar-H), 7.195–7.179 (d, *J*₁ = 8.0 Hz, 2H, Ph-H), 4.024 (s, 3H, CH₃). MS (ESI) calcd for C₂₄H₁₈N₆: 390.16, found: 391.2 (M + H⁺).

6.1.5.9. 2-(1-Benzyl-3-(4-fluorophenyl)-1H-pyrazol-4-yl)-1H-imidazo[4,5-f][1,10]phenanthroline (12a). White crystal; yield: 79.6%; m.p. 208–210 °C; purity by HPLC: 97.4%. ¹H-NMR (DMSO-*d*₆, 500 MHz, ppm): δ13.543 (s, 1H, NH), 9.029–9.017 (dd, *J*₁ = 4.0 Hz, *J*₂ = 1.5 Hz, 2H, Phenanthroline-H), 8.823–8.807 (d, *J*₂ = 8.0 Hz, 1H, Phenanthroline-H), 8.764–8.749 (d, *J*₂ = 7.5 Hz, 1H, Phenanthroline-H), 8.508 (s, 1H, CH), 8.029–7.987 (m, 2H, Ph-H), 7.817–7.804 (m, 2H, Phenanthroline-H), 7.450–7.413 (m, 4H, Ph-H), 7.390–7.346 (m, 1H, Ph-H), 7.264–7.216 (m, 2H, Ph-H), 5.539 (s, 2H, CH₂). ¹³C NMR (DMSO-*d*₆, 125 MHz, ppm): δ162.94, 160.99, 148.02, 147.67, 145.13, 143.39, 136.89, 132.81, 130.22, 130.15, 129.31, 129.29, 128.74, 127.97, 127.90, 123.16, 115.00, 114.83, 110.39, 55.31. MS (ESI) calcd for C₂₉H₁₉FN₆: 470.17, found: 471.2 (M + H⁺).

6.1.5.10. 2-(1-Benzyl-3-(4-chlorophenyl)-1H-pyrazol-4-yl)-1H-imidazo[4,5-f][1,10]phenanthroline (12b). White crystal; yield: 83.7%; m.p. 214–216 °C; purity by HPLC: 99.7%. ¹H-NMR (DMSO-*d*₆, 500 MHz, ppm): δ13.543 (s, 1H, NH), 9.032–9.020 (dd, *J*₁ = 4.0 Hz, *J*₂ = 1.5 Hz, 2H, Phenanthroline-H), 8.828–8.810 (dd, *J*₂ = 8.0 Hz, *J*₁ = 1.0 Hz, 1H, Phenanthroline-H), 8.763–8.745 (dd, *J*₁ = 8.0 Hz, *J*₂ = 1.0 Hz, 1H, Phenanthroline-H), 8.521 (s, 1H, CH), 8.012–7.985 (m, 2H, Ph-H), 7.837–7.794 (m, 2H, Phenanthroline-H), 7.486–7.458 (m, 2H, Ph-H), 7.449–7.412 (m, 4H, Ph-H), 7.390–7.346 (m, 1H, Ph-H), 5.543 (s, 2H, CH₂). ¹³C NMR (CDCl₃-*d*₁+CD₃OD-*d*₄, 125 MHz, ppm): δ148.72, 147.59, 145.08, 143.57, 135.37, 134.04, 132.13, 130.93, 130.03, 130.01, 129.98, 129.96, 129.21, 128.90, 128.45, 128.39, 128.06, 123.05, 110.78, 56.36. MS (ESI) calcd for C₂₉H₁₉ClN₆: 486.14, found: 487.1 (M + H⁺).

6.1.5.11. 2-(1-Benzyl-3-(4-bromophenyl)-1H-pyrazol-4-yl)-1H-imidazo[4,5-f][1,10]phenanthroline (12c). White crystal; yield: 84.3%; m.p. 208–209 °C; purity by HPLC: 99.6%. ¹H-NMR (DMSO-*d*₆, 500 MHz, ppm): δ13.565 (s, 1H, NH), 9.032–9.020 (dd, *J*₁ = 4.5 Hz, *J*₂ = 2.0 Hz, 2H, Phenanthroline-H), 8.820 (br. s, 1H, Phenanthroline-H), 8.768 (br. s, 1H, Phenanthroline-H), 8.525 (s, 1H, CH), 7.952–7.925 (m, 2H, Ph-H), 7.829–7.805 (dd, *J*₁ = 8.0 Hz, *J*₂ = 4.0 Hz, 2H, Phenanthroline-H), 7.621–7.594 (m, 2H, Ph-H), 7.440–7.413 (m, 4H, Ph-H), 7.382–7.355 (m, 1H, Ph-H), 5.543 (s, 2H, CH₂). ¹³C NMR (CDCl₃-*d*₁+CD₃OD-*d*₄, 125 MHz, ppm): δ149.18, 148.74, 147.67,

147.56, 145.01, 143.54, 143.43, 135.37, 132.19, 131.42, 130.04, 129.96, 129.56, 128.92, 128.47, 128.08, 123.09, 122.38, 110.75, 56.39. MS (ESI) calcd for $C_{29}H_{19}BrN_6$: 530.09, found: 531.1 ($M + H^+$).

6.1.5.12. 2-(1-Benzyl-3-(*p*-tolyl)-1*H*-pyrazol-4-yl)-1*H*-imidazo[4,5-*ff*][1,10]phenanthroline (**12d**). White crystal; yield: 77.3%; m.p. 206–208 °C; purity by HPLC: 99.9%. 1H -NMR (DMSO- d_6 , 500 MHz, ppm): δ 13.545 (s, 1H, NH), 9.026–9.018 (m, 2H, Phenanthroline-H), 8.830–8.814 (d, $J_1 = 8.0$ Hz, 1H, Phenanthroline-H), 8.766–8.750 (d, $J_1 = 8.0$ Hz, 1H, Phenanthroline-H), 8.468 (s, 1H, CH), 7.810–7.772 (m, 4H, Ar-H), 7.438–7.410 (m, 4H, Ph-H), 7.376–7.342 (m, 1H, Ph-H), 7.185–7.169 (d, $J_1 = 8.0$ Hz, 2H, Ph-H), 5.522 (s, 2H, CH_2), 2.300 (s, 3H, CH_3). ^{13}C NMR (CDCl $_3$ - d_1 +CD3OD- d_4 , 125 MHz, ppm): δ 149.68, 147.77, 145.39, 143.66, 138.45, 135.46, 132.00, 129.80, 129.72, 129.67, 129.30, 128.90, 128.41, 128.17, 128.12, 128.08, 128.01, 123.05, 110.63, 56.35, 21.19. MS (ESI) calcd for $C_{30}H_{22}N_6$: 466.19, found: 467.2 ($M + H^+$).

6.1.5.13. 3-(3-(4-fluorophenyl)-4-(1*H*-imidazo[4,5-*ff*][1,10]phenanthrolin-2-yl)-1*H*-pyrazol-1-yl)-*N,N*-dimethylpropan-1-amine (**13a**). White crystal; yield: 65.3%; m.p. 284–286 °C; purity by HPLC: 96.2%. 1H -NMR (DMSO- d_6 , 500 MHz, ppm): δ 13.527 (s, 1H, NH), 9.034–9.022 (dd, $J_1 = 4.0$ Hz, $J_2 = 2.0$ Hz, 2H, Phenanthroline-H), 8.802 (br. s, 2H, Phenanthroline-H), 8.438 (s, 1H, CH), 8.036–8.001 (m, 2H, Ph-H), 7.830–7.808 (m, 2H, Phenanthroline-H), 7.269–7.222 (m, 2H, Ph-H), 4.320–4.292 (t, $J_1 = 7.0$ Hz, 2H, CH_2), 2.325–2.298 (t, $J_1 = 6.75$ Hz, 2H, CH_2), 2.187 (s, 6H, CH_3), 2.085–2.030 (m, 2H, CH_2). MS (ESI) calcd for $C_{27}H_{24}FN_7$: 465.21, found: 466.2 ($M + H^+$).

6.1.5.14. 3-(3-(4-chlorophenyl)-4-(1*H*-imidazo[4,5-*ff*][1,10]phenanthrolin-2-yl)-1*H*-pyrazol-1-yl)-*N,N*-dimethylpropan-1-amine (**13b**). White crystal; yield: 68.9%; m.p. 264–265 °C; purity by HPLC: 96.2%. 1H -NMR (DMSO- d_6 , 500 MHz, ppm): δ 13.550 (s, 1H, NH), 9.036–9.024 (dd, $J_1 = 4.5$ Hz, $J_2 = 2.0$ Hz, 2H, Phenanthroline-H), 8.807 (br. s, 2H, Phenanthroline-H), 8.458 (s, 1H, CH), 8.033–8.006 (m, 2H, Ph-H), 7.825 (br. s, 2H, Phenanthroline-H), 7.493–7.466 (m, 2H, Ph-H), 4.327–4.299 (t, $J_1 = 7.0$ Hz, 2H, CH_2), 2.334–2.307 (t, $J_1 = 6.75$ Hz, 2H, CH_2), 2.193 (s, 6H, CH_3), 2.089–2.033 (m, 2H, CH_2). MS (ESI) calcd for $C_{27}H_{24}ClN_7$: 481.18, found: 482.2 ($M + H^+$).

6.1.5.15. 3-(3-(4-bromophenyl)-4-(1*H*-imidazo[4,5-*ff*][1,10]phenanthrolin-2-yl)-1*H*-pyrazol-1-yl)-*N,N*-dimethylpropan-1-amine (**13c**). White crystal; yield: 69.1%; m.p. 237–238 °C; purity by HPLC: 97.6%. 1H -NMR (DMSO- d_6 , 500 MHz, ppm): δ 13.546 (s, 1H, NH), 9.034–9.028 (dd, $J_1 = 3.0$ Hz, $J_2 = 2.0$ Hz, 2H, Phenanthroline-H), 8.833–8.818 (d, $J_1 = 4.5$ Hz, 1H, Phenanthroline-H), 8.795–8.780 (d, $J_1 = 4.5$ Hz, 1H, Phenanthroline-H), 8.459 (s, 1H, CH), 7.966–7.949 (d, $J_1 = 8.5$ Hz, 2H, Ph-H), 7.824 (br. s, 2H, Phenanthroline-H), 7.624–7.607 (d, $J_1 = 8.5$ Hz, 2H, Ph-H), 4.329–4.301 (t, $J_1 = 7.0$ Hz, 2H, CH_2), 2.365–2.341 (t, $J_1 = 6.0$ Hz, 2H, CH_2), 2.217 (s, 6H, CH_3), 2.098–2.043 (m, 2H, CH_2). MS (ESI) calcd for $C_{27}H_{24}BrN_7$: 525.13, found: 526.1 ($M + H^+$).

6.1.5.16. 3-(4-(1*H*-imidazo[4,5-*ff*][1,10]phenanthrolin-2-yl)-3-(*p*-tolyl)-1*H*-pyrazol-1-yl)-*N,N*-dimethylpropan-1-amine (**13d**). White crystal; yield: 62.3%; m.p. 232–234 °C; purity by HPLC: 96.6%. 1H -NMR (DMSO- d_6 , 500 MHz, ppm): δ 13.504 (s, 1H, NH), 9.034–9.022 (dd, $J_1 = 4.5$ Hz, $J_2 = 2.0$ Hz, 2H, Phenanthroline-H), 8.819–8.784 (m, 2H, Phenanthroline-H), 8.380 (s, 1H, CH), 7.830–7.804 (m, 2H, Phenanthroline-H), 7.799–7.783 (d, $J_1 = 8.0$ Hz, 2H, Ph-H), 7.193–7.177 (d, $J_1 = 8.0$ Hz, 2H, Ph-H), 4.306–4.278 (t, $J_1 = 7.0$ Hz, 2H, CH_2), 2.323–2.296 (t, $J_1 = 6.75$ Hz, 5H, CH_2 , CH_3), 2.184 (s, 6H, CH_3), 2.078–2.022 (m, 2H, CH_2). MS (ESI) calcd for

$C_{28}H_{27}N_7$: 461.23, found: 462.2 ($M + H^+$).

6.1.5.17. 2-(1-(2,4-dinitrophenyl)-3-(4-fluorophenyl)-1*H*-pyrazol-4-yl)-1*H*-imidazo[4,5-*ff*][1,10]phenanthroline (**14a**). Yellow solid; yield: 86.8%; m.p. >310 °C; purity by HPLC: 97.1%. 1H -NMR (DMSO- d_6 , 500 MHz, ppm): δ 13.917 (s, 1H, NH), 9.243 (s, 1H, Ph-H), 9.072–9.060 (dd, $J_1 = 4.0$ Hz, $J_2 = 1.5$ Hz, 2H, Phenanthroline-H), 8.992–8.987 (d, $J_1 = 2.5$ Hz, 1H, Ph-H), 8.862 (br. s, 1H, Phenanthroline-H), 8.827 (br. s, 1H, Phenanthroline-H), 8.759–8.736 (dd, $J_1 = 9.0$ Hz, $J_2 = 2.5$ Hz, 1H, Ph-H), 8.332–8.314 (d, $J_1 = 9.0$ Hz, 1H, CH), 7.942–9.901 (m, 2H, Ph-H), 7.893–7.868 (m, 2H, Phenanthroline-H), 7.340–7.292 (m, 2H, Ph-H). MS (ESI) calcd for $C_{28}H_{15}FN_8O_4$: 546.12, found: 547.1 ($M + H^+$).

6.1.5.18. 2-(3-(4-chlorophenyl)-1-(2,4-dinitrophenyl)-1*H*-pyrazol-4-yl)-1*H*-imidazo[4,5-*ff*][1,10]phenanthroline (**14b**). Yellow solid; yield: 88.6%; m.p. >310 °C; purity by HPLC: 98.18%. 1H -NMR (DMSO- d_6 , 500 MHz, ppm): δ 13.867 (s, 1H, NH), 9.238 (s, 1H, Ph-H), 9.058–9.050 (d, $J_1 = 4.0$ Hz, 2H, Phenanthroline-H), 8.994–8.989 (d, $J_1 = 2.5$ Hz, 1H, Ph-H), 8.868–8.853 (d, $J_1 = 7.5$ Hz, 1H, Ph-H), 8.767–8.738 (m, 2H, Phenanthroline-H), 8.332–8.314 (d, $J_1 = 9.0$ Hz, 1H, CH), 7.899–9.882 (d, $J_1 = 8.5$ Hz, 2H, Ph-H), 7.864–7.824 (m, 2H, Phenanthroline-H), 7.551–7.534 (d, $J_1 = 8.5$ Hz, 2H, Ph-H). MS (ESI) calcd for $C_{28}H_{15}ClN_8O_4$: 562.09, found: 563.3 ($M + H^+$).

6.1.5.19. 2-(3-(4-bromophenyl)-1-(2,4-dinitrophenyl)-1*H*-pyrazol-4-yl)-1*H*-imidazo[4,5-*ff*][1,10]phenanthroline (**14c**). Yellow Solid; yield: 89.1%; m.p. >310 °C; purity by HPLC: 96.4%. 1H -NMR (DMSO- d_6 , 500 MHz, ppm): δ 13.866 (s, 1H, NH), 9.232 (s, 1H, Ph-H), 9.055–9.044 (dd, $J_1 = 4.0$ Hz, $J_2 = 1.5$ Hz, 2H, Phenanthroline-H), 8.989–8.984 (d, $J_1 = 2.5$ Hz, 1H, Ph-H), 8.867–8.852 (d, $J_1 = 7.5$ Hz, 1H, Ph-H), 8.763–8.731 (m, 2H, Phenanthroline-H), 8.330–8.312 (d, $J_1 = 9.0$ Hz, 1H, CH), 7.846–7.816 (m, 4H, Ar-H), 7.861–7.664 (m, 2H, Ph-H). MS (ESI) calcd for $C_{28}H_{15}BrN_8O_4$: 606.04, found: 607.3 ($M + H^+$).

6.1.5.20. 2-(1-(2,4-dinitrophenyl)-3-(*p*-tolyl)-1*H*-pyrazol-4-yl)-1*H*-imidazo[4,5-*ff*][1,10]phenanthroline (**14d**). Yellow solid; yield: 82.3%; m.p. >310 °C; purity by HPLC: 98.3%. 1H -NMR (DMSO- d_6 , 500 MHz, ppm): δ 13.860 (s, 1H, NH), 9.210 (s, 1H, Ph-H), 9.061–9.049 (dd, $J_1 = 4.5$ Hz, $J_2 = 2.0$ Hz, 2H, Phenanthroline-H), 8.981–8.975 (d, $J_1 = 3.0$ Hz, 1H, Ph-H), 8.870–8.856 (d, $J_1 = 7.0$ Hz, 1H, Ph-H), 8.775–8.759 (d, $J_1 = 7.0$ Hz, 1H, Phenanthroline-H), 8.741–8.718 (dd, $J_1 = 9.0$ Hz, $J_2 = 2.5$ Hz, 1H, Phenanthroline-H), 8.322–8.304 (d, $J_1 = 9.0$ Hz, 1H, CH), 7.860–7.827 (m, 2H, Phenanthroline-H), 7.701–7.684 (d, $J_1 = 8.5$ Hz, 2H, Ph-H), 7.242–7.226 (d, $J_1 = 8.0$ Hz, 2H, Ph-H), 2.314 (s, 3H, CH_3). MS (ESI) calcd for $C_{29}H_{18}N_8O_4$: 542.15, found: 543.2 ($M + H^+$).

6.1.5.21. 6-(3-(4-bromophenyl)-4-(1*H*-imidazo[4,5-*ff*][1,10]phenanthrolin-2-yl)-1*H*-pyrazol-1-yl)pyridazin-3-amine (**15**). Yellow solid; yield: 77.4%; m.p. >310 °C; purity by HPLC: 96.9%. 1H -NMR (DMSO- d_6 , 500 MHz, ppm): δ 9.174 (s, 1H, Pyridazine-H), 9.055 (br. s, 2H, Phenanthroline-H), 8.827 (br. s, 2H, Phenanthroline-H), 8.221 (s, 1H, CH), 8.197–8.182 (d, $J_1 = 7.5$ Hz, 2H, Ph-H), 7.901 (br. s, 2H, Phenanthroline-H), 7.727–7.712 (d, $J_1 = 7.5$ Hz, 2H, Ph-H), 7.215–7.196 (d, $J_1 = 9.5$ Hz, 1H, Pyridazine-H). MS (ESI) calcd for $C_{26}H_{16}BrN_9$: 533.07, found: 535.1 ($M + 2H^+$).

6.2. Cytotoxicity assay

The cytotoxicity in vitro of synthesized compounds **10–15** was evaluated by Cell Counting Kit-8 assay (DOJINDO, Kumamoto, Japan) [47] on human lung adenocarcinoma and human fetal lung

fibroblast cell lines: A549 and MRC-5. Cisplatin and leading compound **2** were used as positive controls. Initially, cells were routinely cultured in RPMI 1640 (Invitrogen Gibco) supplemented with 10% FBS (Invitrogen Gibco) and penicillin-streptomycin (Sigma-Aldrich, 100 U/mL) at 37.0 °C in a humidified atmosphere containing 5% CO₂. Moreover, 95 µL cell suspensions were seeded at 5000 cells per well in 96 well plates for 24 h to culture. After that, 5 µL solution of compounds (1 µL of a solution of compounds in DMSO was diluted with 4 µL culture medium) was mixed into the 96 well plates sequentially to culture for 36 h. Then 10 µL CCK8 reagents were added to each well and incubated at 37 °C for 1 h. Finally, the optical density of each sample was measured at 450 nm using a microplate reader (Molecular Devices M4).

6.3. Electrophoretic mobility shift assay (EMSA)

DNA samples (2 µM) were prepared in a buffer (pH 7.4) containing 10 mM Tris–HCl, 10 mM KCl, 0.1 mM EDTA in the presence and absence of compounds were incubated for 24 h after annealing at 95 °C. The electrophoretic mobility shift assay (EMSA) was conducted using 16% native polyacrylamide gel electrophoresis and 1 × TBE (Tris base-boric acid-EDTA) buffer solution. The gels were run at 150 V for 4 h in 4 °C circulating cooling water. The gels were then immersed in 1 × SYBR Gold and in 1 × TE solution for 30 min, respectively, rinsed with ultrapure water, and then photographed using a Bio-Rad gel imaging analyzer.

6.4. UV melting assay

Temperature-dependent absorption was measured using a UV-2550 spectrophotometer (Shimadzu) equipped with a thermoelectrically controlled cell holder and quartz cells with a path length of 10 mm. The absorbance at 295 nm for 2 µM G-rich DNAs and at 260 nm for 2 µM double-stranded DNA (ds-DNA) in a buffer (pH 7.4) containing 10 mM Tris–HCl, 10 mM KCl, 0.1 mM EDTA, in the absence and presence of compounds (20 µM) and the buffer as a reference was monitored with the temperature being ramped between 1 °C and 95 °C at 1.0 °C/min, the samples being allowed to equilibrate for 10 min at each temperature setting. The obtained curve shows the melting profiles. By using UV-melting analysis system, shape analysis of the melting curves yielded transition temperatures (T_m), which are the midpoint temperatures of the helix–coil transitions. The melting profiles for the quadruplex formed by the telomeric DNA were acquired at 295 nm. Dry nitrogen was passed through the sample chamber to prevent condensation.

6.5. Wound healing assay

A549 cells were grown in DMEM medium containing growth factors at the cell density of 1 × 10⁵ cells/mL for 24 h. A disposable 200 µL plastic pipette tip was used to scratch the monolayer of cells in a streaking motion. Compounds were added to the streaked cell culture at the indicated concentrations. The streaked cells were then cultured in serum-free medium for an additional 48 h and photographed. To quantify the experimental results, the % cell inhibitory rate was calculated by the equation [45]: cell inhibitory rate (%) = (1 - D_{drug}/D_{control}) × 100%, where D_{drug} is mean distance of cell migration in drug group, D_{control} is mean distance of cell migration in control group, with pictures of the initial wounded monolayers being compared with the corresponding pictures of cells at the end of the incubation, and data are presented as mean ± SD. Artificial lines fitting the cutting edges were drawn on pictures of the original wounds and on the pictures of cultures after incubation. Three different points were marked on each plate.

Representative images of three independent experiments were shown.

Acknowledgment

We gratefully acknowledge the financial support from National Natural Science Foundation of China (21572207), Program of International S & T Cooperation (2015DFG32530), Zhejiang Provincial Natural Science Foundation of China (LY16160003).

Appendix A. Supplementary data

Supplementary data related to this article can be found at <http://dx.doi.org/10.1016/j.ejmech.2017.03.030>.

References

- [1] A. Jemal, R. Siegel, J. Xu, E. Ward, Cancer statistics, 2010, CA, Cancer. J. Clin. 60 (2010) 277–300.
- [2] J.D. Minna, J.A. Roth, A.F. Gazdar, Focus on lung cancer, Cancer Cell. 1 (2002) 49–52.
- [3] P.C. Hoffman, A.M. Mauer, E.E. Vokes, Lung cancer, Lancet 355 (2000) 479–485.
- [4] R. Siegel, D. Naishadham, A. Jemal, Cancer statistics, CA, Cancer. J. Clin. 63 (2013) 11–30.
- [5] J.M. Varlotto, L.N. Medford-Davis, A. Recht, J.C. Flickinger, E. Schaefer, M.M. DeCamp, Failure rates and patterns of recurrence in patients with respected N1 non-small-cell lung cancer, Int. J. Rad. Onc., Biol. Phys. 81 (2011) 353–359.
- [6] P. Saintigny, J.A. Burger, Recent advances in non-small cell lung cancer biology and clinical management, Discov. Med. 13 (2012) 287–297.
- [7] N. van Zandwijk, Neoadjuvant strategies for non-small cell lung cancer, Lung Cancer 34 (2001) 145–150.
- [8] H. Narang, A. Kumar, N. Bhat, B.N. Pandey, A. Ghosh, Effect of proton and gamma irradiation on human lung carcinoma cells: gene expression, cell cycle, cell death, epithelial–mesenchymal transition and cancer-stem cell trait as biological end points, Mutat. Res. 780 (2015) 35–46.
- [9] S. Dasari, P.B. Tchounwou, Cisplatin in cancer therapy: molecular mechanisms of action, Eur. J. Pharmacol. 740 (2014) 364–378.
- [10] S. Kobayashi, T.J. Boggon, T. Dayaram, P.A. Janne, O. Kocher, M. Meyerson, EGFR mutation and resistance of non-small-cell lung cancer to gefitinib, N. Engl. J. Med. 352 (2005) 786–792.
- [11] J.A. Engelman, K. Zejnullahu, T. Mitsudomi, Y. Song, C. Hyland, J.O. Park, MET amplification leads to gefitinib resistance in lung cancer by activating ERBB3 signaling, Science 316 (2007) 1039–1043.
- [12] W.J. Zheng, C.W. Cao, Y.N. Liu, Q.Q. Yu, C.P. Zheng, D.D. Sun, X.F. Ren, J. Liu, Multifunctional polyamidoamine-modified selenium nanoparticles dual-delivering siRNA and cisplatin to A549/DDP cells for reversal multidrug resistance, Acta Biomater. 11 (2015) 368–380.
- [13] W.C. Dempke, T. Suto, M. Reck, Targeted therapies for non-small cell lung cancer, Lung Cancer 67 (2010) 257–274.
- [14] R.K. Moyzis, J.M. Buckingham, L.S. Cram, M. Dani, L.L. Deaven, M.D. Jones, J. Meyne, R.L. Ratliff, J.R. Wu, A highly conserved repetitive DNA-sequence, (ttagg)_n, present at the telomeres of human-chromosomes, Proc. Nat. Acad. Sci. U. S. A. 85 (1988) 6622–6626.
- [15] J.A. Zhou, G. Yuan, Specific recognition of human telomeric G-quadruplex DNA with small molecules and the conformational analysis by esi mass spectrometry and circular dichroism spectropolarimetry, Chem. Eur. J. 13 (2007) 5018–5023.
- [16] S. Neidle, Human telomeric G-quadruplex: the current status of telomeric Quadruplexes as therapeutic targets in human cancer, FEBS. J. 277 (2010) 1118–1125.
- [17] Y. Xu, Y.T. Suzuki, T. Ishizuka, C.D. Xiao, X. Liu, T. Hayashi, M. Komiyama, Finding a human telomere DNA–RNA hybrid G-quadruplex formed by human telomeric 6-mer RNA and 16-mer DNA using click chemistry: a protective structure for telomere end, Bioorgan. Med. Chem. 22 (2014) 4419–4421.
- [18] (a) E.H. Blackburn, Switching and signaling at the telomere, Cell. 106 (2001) 661–673; (b) T. de Lange, T-loops and the origin of telomeres, Nat. Rev. Mol. Cell Biol. 5 (2004) 323–329.
- [19] C.M. Gao, W. Zhang, S.N. He, S.F. Li, F. Liu, Y.Y. Jiang, Synthesis and anti-proliferative activity of 2,7-diamino 10-(3,5-dimethoxy)benzyl-9(10H)-acridone derivatives as potent telomeric G-quadruplex DNA ligands, Bioorg. Chem. 60 (2015) 30–36.
- [20] D.E. Gomez, R.G. Armando, H.G. Farina, P.L. Menna, C.S. Cerrudo, P.D. Ghiringhelli, D.F. Alonso, Telomere structure and telomerase in health and disease, Int. J. Oncol. 41 (2012) 1561–1569.
- [21] D.L.M. Gómez, H.G. Farina, D.E. Gómez, Telomerase regulation: a key to inhibition, Int. J. Oncol. 43 (2013) 1351–1356.
- [22] X.B. Sui, N. Kong, Z.G. Wang, H.M. Pan, Epigenetic regulation of the human

- telomerase reverse transcriptase gene: a potential therapeutic target for the treatment of leukemia, *Oncol. Lett.* 6 (2013) 317–322.
- [23] W.B. Chen, L.J. Qin, S.S. Wang, M. Li, D.B. Shi, Y. Tian, J.S. Wang, L.Y. Fu, Z.L. Li, W. Guo, W.D. Yu, Y.H. Yuan, T.B. Kang, W.L. Huang, W.G. Deng, CPSF4 activates telomerase reverse transcriptase and predicts poor prognosis in human lung adenocarcinomas, *Mol. Oncol.* 8 (2014) 704–716.
- [24] M. Balaz, M.D. Napoli, A.E. Holmes, A. Mammana, K. Nakanishi, N. Berova, R. Purrello, A cationic zinc porphyrin as a chiroptical sensor for Z-DNA, *Angew. Chem.* 44 (2005) 4006–4009.
- [25] R.D. Wells, Non-B DNA conformations, mutagenesis and disease, *Trends biochem. Sci.* 32 (2007) 271–278.
- [26] R.D. Wells, Discovery of the role of non-B DNA structures in mutagenesis and human genomic disorders, *J. Biol. Chem.* 14 (2009) 8997–9009.
- [27] Y. Jiang, A.C. Chen, G.T. Kuang, S.K. Wang, T.M. Ou, J.H. Tan, D. Li, Z.S. Huang, Design, synthesis and biological evaluation of 4-anilinoquinazoline derivatives as new c-myc G-quadruplex ligands, *Eur. J. Med. Chem.* 122 (2016) 264–279.
- [28] A. Bugaut, P. Alberti, Understanding the stability of DNA G-quadruplex units in long human telomeric strands, *Biochimie* 113 (2015) 125–133.
- [29] K. Nalapareddy, H. Jiang, L.M.G. Gutierrez, K.L. Rudolph, Determining the influence of telomere dysfunction and DNA damage on stem and progenitor cell aging—what markers can we use? *Exp. Gerontol.* 43 (2008) 998–1004.
- [30] F. Palluotto, A. Sosic, O. Pinato, G. Zoidis, M. Catto, C. Sissi, B. Gatto, A. Carotti, Quinolino[3,4-b]quinoxalines and pyridazino[4,3-c]quinoline derivatives: synthesis, inhibition of topoisomerase IIa, G-quadruplex binding and cytotoxic properties, *Eur. J. Med. Chem.* 123 (2016) 704–717.
- [31] C.H. Wang, B. Carter-Cooper, Y.X. Du, J. Zhou, M.A. Saeed, J.B. Liu, M. Guo, B. Roembke, C. Mikek, E.A. Lewis, R.G. Lapidus, H.O. Sintim, Alkyne-substituted diminazene as G-quadruplex binders with anticancer activities, *Eur. J. Med. Chem.* 118 (2016) 266–275.
- [32] J. Kobayashi, J.F. Cheng, H. Nakamura, Y. Ohizumi, Y. Hirata, T. Sasaki, T. Ohta, S. Nozoa, Ascididemin, a novel pentacyclic aromatic alkaloid with potent antileukemic activity from Okinawan tunicate *Didemnum* sp, *Tetrahedron Lett.* 29 (1988) 1177–1180.
- [33] S.S. Matsumoto, M.H. Sidford, J.A. Holden, L.R. Barrows, B.R. Copp, Mechanism of action studies of cytotoxic marine alkaloids: ascididemin exhibits thiol-dependent oxidative DNA cleavage, *Tetrahedron Lett.* 41 (2000) 1667–1670.
- [34] E. Delfourne, F. Darro, P. Portefaix, C. Galaup, S. Bayssade, A. Bouteillé, L. Le Corre, J. Bastide, F. Collignon, B. Lesur, A. Frydman, R. Kiss, Synthesis and in vitro antitumor activity of novel ring D analogues of the marine pyridoacridine ascididemin: structure-activity relationship, *J. Med. Chem.* 45 (2002) 3765–3771.
- [35] G. Chelucci, R. Thummel, P. Chem, Chiral 2,2'-bipyridines, 1,10-phenanthrolines, and 2,2': 6', 2"-terpyridines: syntheses and applications in asymmetric homogeneous catalysis, *Rev.* 102 (2002) 3129–3170.
- [36] J. Liu, W. Zheng, S. Shi, C. Tan, J. Chen, K. Zheng, L. Ji, Synthesis, antitumor activity and structure-activity relationships of a series of Ru(II) complexes, *J. Inorg. Biochem.* 102 (2008) 193–202.
- [37] E. Meggers, Targeting proteins with metal complexes, *Chem. Commun.* (2009) 1001–1010.
- [38] E. Shirakawa, K. Itoh, T. Higashino, T. Hayashi, tert-Butoxide-Mediated arylation of benzene with aryl halides in the presence of a catalytic 1,10-phenanthroline derivative, *J. Am. Chem. Soc.* 132 (2010) 15537–15539.
- [39] M. Kaplanisa, G. Stamatakis, V.D. Papakonstantinou, M.P. Petsotas, C.A. Demopoulos, C.A. Mitsopoulou, Re(I) tricarbonyl complex of 1,10-phenanthroline-5,6-dione: DNA binding, cytotoxicity, anti-inflammatory and anti-coagulant effects towards platelet activating factor, *J. Inorg. Biochem.* 135 (2014) 1–9.
- [40] C.Y. Wei, J.H. Wang, Y. Wen, J. Liu, L.H. Wang, 4-(1*H*-imidazo[4,5-*f*]-1,10-phenanthroline-2-yl)phenol-based G-quadruplex DNA binding agents: telomerase inhibition, cytotoxicity and DNA-binding studies, *Bioorgan. Med. Chem.* 21 (2013) 3379–3387.
- [41] M.C. Nielsen, A.F. Larsen, F.H. Abdikadir, T. Ulven, Phenanthroline-2,9-bis-triazoles as selective G-quadruplex ligands, *Eur. J. Med. Chem.* 72 (2014) 119–126.
- [42] S.S. Qasim, S.S. Ali, S.K. Ahmed, SnCl₂·2H₂O catalyzed one-pot synthesis of 2-phenylimidazo [4,5-*f*] [1,10] phenanthroline, *Res. J. Pharm. Biol. Chem. Sci.* 2 (2011) 423–428.
- [43] D.D. Sun, W.Z. Wang, J.W. Mao, W.J. Mei, J. Liu, Imidazo [4,5-*f*] [1,10] phenanthroline derivatives as inhibitor of c-myc gene expression in A549 cells via NF- κ B pathway, *Bioorg. Med. Chem. Lett.* 22 (2012) 102–105.
- [44] A.F. Sherif Rostom, A.S. Manal, M.A. El-Demellawy, Polysubstituted pyrazoles, part 5.¹ Synthesis of new 1-(4-chlorophenyl)-4-hydroxy-1*H*-pyrazole-3-carboxylic acid hydrazide analogs and some derived ring systems. A novel class of potential antitumor and anti-HCV agents, *Eur. J. Med. Chem.* 38 (2003) 959–974.
- [45] W. Zhang, M. Chen, Y.L. Wu, Y. Tanaka, Y.J. Ji, S.L. Zhang, C.H. Wei, Y. Xu, Formation and stabilization of the telomeric antiparallel G-quadruplex and inhibition of telomerase by novel benzothioxanthene derivatives with antitumor activity, *Sci. Rep.* 5 (2015) 13693, <http://dx.doi.org/10.1038/srep13693>.
- [46] Y.X. Xiong, Z.S. Huang, J.H. Tan, Targeting G-quadruplex nucleic acids with heterocyclic alkaloids and their derivatives, *Eur. J. Med. Chem.* 97 (2015) 538–551.
- [47] Y. Yan, J. Tan, T. Ou, Z. Huang, L. Gu, DNA G-quadruplex binders: a patent review, *Expert Opin. Ther. Pat.* 23 (2013) 1495–1509.
- [48] A.V. Lebedev, A.B. Lebedeva, V.D. Sheludyakov, E.A. Kovaleva, O.L. Ustinova, I.B. Kozhevnikov, Synthesis of 3-substituted arylpyrazole-4-carboxylic acids, *Russ. J. Gen. Chem.* 75 (2005) 782–789.
- [49] L.L. Xu, C.J. Zheng, L.P. Sun, J. Miao, H.R. Piao, Synthesis of novel 1,3-diaryl pyrazole derivatives bearing rhodanine-3-fatty acid moieties as potential antibacterial agents, *Eur. J. Med. Chem.* 48 (2012) 174–178.
- [50] C.F. Zhong, H.L. Huang, A.H. He, H.L. Zhang, Synthesis and luminescent properties of novel polymeric metal complexes with bis(1,10-phenanthroline) group, *Dyes Pigments* 77 (2008) 578–583.
- [51] T. Thierry, G. Christophe, M. Jose, P.C. Michel, G. Alain, V. Patrice, Synthesis of 2-substituted-3-nitroimidazo[1,2-*b*]pyridazines as potential biologically active agents, *J. Heterocycl. Chem.* 39 (2002) 173–177.
- [52] F. Xue, L. Hu, R.L. Ge, L.X. Yang, K. Liu, Y.Y. Li, Y.F. Sun, K. Wang, Autophagy-deficiency in hepatic progenitor cells leads to the defects of stemness and enhances susceptibility to neoplastic transformation, *Cancer Lett.* 371 (2016) 38–47.
- [53] C. Sissi, Tri-, Tetra- and heptacyclic perylene analogues as new potential antineoplastic agents based on DNA telomerase inhibition, *Bioorg. Med. Chem.* 15 (2007) 555–562.
- [54] F. Cuenca, O. Greciano, M. Gunaratnam, S. Haider, D. Munnur, R. Nanjunda, W.D. Wilson, S. Neidle, Tri and tetra-substituted naphthalene diimides as potent G-quadruplex ligands, *Bioorg. Med. Chem. Lett.* 18 (2008) 1668–1673.
- [55] J.L. Mergny, A.T. Phan, L. Lacroix, Following G-quartet formation by UV-spectroscopy, *FEBS Lett.* 435 (1998) 74–78.
- [56] P.A. Rachwal, K.R. Fox, Quadruplex melting, *Methods* 43 (2007) 291–301.
- [57] L. Ying, J.J. Green, H. Li, D. Klenerman, S. Balasubramanian, Studies on the structure and dynamics of the human telomeric G-quadruplex by single-molecule fluorescence resonance energy transfer, *Proc. Natl. Acad. Sci. U. S. A.* 100 (2003) 14629–14634.
- [58] A.T. Phan, J.L. Mergny, Human telomeric DNA: G-quadruplex, i-motif and Watson-Crick double helix, *Nucleic acids Res.* 30 (2002) 4618–4625.